

Testing Anomalous Gauge Couplings of the Higgs Boson via Weak-Boson Scatterings at the LHC

Bin Zhang

Department of Physics, Tsinghua University, Beijing 100084, China.

Yu-Ping Kuang

*China Center of Advanced Science and Technology (World Laboratory), P.O.Box 8730, Beijing 100080, China;
Department of Physics, Tsinghua University, Beijing 100084, China.**

Hong-Jian He

Center for Particle Physics, University of Texas at Austin, Austin, Texas 78712, U.S.A.

C.-P. Yuan

*Department of Physics and Astronomy, Michigan State University, East Lansing, MI 48824, U.S.A.
(TUHEP-TH-01127, UTHEP-03-13, MSUHEP-030103)*

We propose a sensitive way to test the anomalous HVV couplings ($V = W^\pm, Z^0$) of the Higgs boson (H^0), which can arise from either the dimension-3 effective operator in a nonlinearly realized Higgs sector or the dimension-6 effective operators in a linearly realized Higgs sector, via the VV scattering channels at the CERN LHC. The gold-plated pure leptonic decay modes of the final state weak bosons in the processes $pp \rightarrow VVjj$ are studied. For comparison, we also analyze the constraints from the precision electroweak data, the expected precision of the measurements of the Higgs production rate, decay width and branching ratios at the Tevatron Run-2 and the LHC, and the requirement of the unitarity of the S -matrix. We show that, with an integrated luminosity of 300 fb^{-1} and sufficient kinematical cuts for suppressing the backgrounds, studying the process $pp \rightarrow W^+W^+jj \rightarrow \ell^+\nu\ell^+\nu jj$ can probe the anomalous HWW couplings at a few tens of percent level for the nonlinearly realized Higgs sector, and at the level of $0.01 - 0.08 \text{ TeV}^{-1}$ for the linearly realized effective Lagrangian.

PACS number(s): 14.65.Ha, 12.15.Lk, 12.60.Nz

I. INTRODUCTION

The Standard Model (SM) of the electroweak interactions has proved to be very successful in explaining all the available experimental data at the scale $\lesssim \mathcal{O}(100) \text{ GeV}$. However, the mechanism of the electroweak symmetry breaking (EWSB) remains as one of the most profound puzzles in particle physics. The Higgs sector of the SM suffers the well-known problems of triviality [1] and unnaturalness [2], therefore there has to be new physics beyond the SM above certain high energy scale Λ . Within the SM formalism, so far the precision electroweak data favors a light Higgs boson. If a light Higgs boson candidate H^0 is found in the future collider experiments, such as the Run-2 of the Fermilab Tevatron or the CERN Large Hadron Collider (LHC), the next important task is to experimentally measure the gauge interactions of this Higgs

scalar and verify the nature of the EWSB mechanism. The detection of the anomalous gauge couplings of the Higgs boson will point to the new physics underlying the EWSB that goes beyond the minimal SM Higgs mechanism.

Although the correct theory of new physics is not yet clear, the effect of any new physics at energy below the cutoff scale Λ can be parametrized as effective interactions in an effective theory whose particle content is the same as the SM. This provides a model-independent description, and the anomalous couplings relative to that of the SM reflect the virtual contributions from the new physics. In the present study, we assume that all possible Higgs scalars other than the lightest Higgs boson H^0 are heavy and around or above the scale Λ , so that only H^0 is relevant to the effective theory. Therefore, testing the effective anomalous gauge couplings of the Higgs boson can discriminate

the new physics effects in the EWSB sector from that of the SM. It has been pointed out that sensitive tests of the anomalous HVV couplings (with $V = W^\pm, Z^0$) can be performed via Higgs boson productions at the future high energy linear colliders [3]. The tests of the anomalous HVV couplings at hadron colliders via the decay mode $H \rightarrow \gamma\gamma$ and $H \rightarrow \tau\tau$ have also been studied, and the obtained sensitivities are lower than that at the LC [4–6].

In this paper, following our recent proposal [7], we study an additional way to test the anomalous HVV couplings via the weak-boson scatterings at the LHC. We will show that at the LHC, rather sensitive tests of the anomalous HVV couplings can be obtained by measuring the cross sections of the longitudinal weak-boson scattering, $V_L V_L \rightarrow V_L V_L$ ($V_L = W_L^\pm, Z_L^0$), especially $W_L^+ W_L^+ \rightarrow W_L^+ W_L^+$. The scattering amplitude contains two parts: (a) the amplitude $T(V, \gamma)$ related only to the electroweak gauge bosons as shown in Fig. 1(a), and (b) the amplitude $T(H)$ related to the Higgs boson as shown in Fig. 1(b). In the SM, the HVV coupling constant is fixed to be the same as the non-Abelian gauge self-coupling of the weak bosons. At high energies, both $T(V, \gamma)$ and $T(H)$ contain a piece increasing with the center-of-mass energy (E) as E^2 in the nonlinear realization and as E^4 in the linear realization. However, in the SM, the E^4 -dependent pieces from (s, t, u)-channels are all absent because it contains interactions only up to dimension-4; and the two E^2 -dependent pieces precisely cancel with each other in the sum $T(V, \gamma) + T(H)$, resulting in the expected E^0 -behavior for the total amplitude, as required by the unitarity of the SM S -matrix. If the HVV couplings are anomalous due to the new physics above the scale Λ , the new E^2 - or E^4 -dependent pieces will not cancel and the total amplitude will behave as E^2 or E^4 in the high energy regions below Λ . Such deviations from the E^0 behavior of the SM amplitude can provide rather sensitive test of the anomalous HVV couplings in high energy VV scattering experiments. This type of tests require neither the detection of the Higgs boson resonance nor the measurement of the Higgs boson decay branching ratios, and is thus of special interest. If the anomalous HVV coupling associated with new physics effect is rather large, the total width of H may become so large that H cannot be detected as a sharp resonance [8] and therefore escapes the detection when scanning the invariant mass of its decay products around m_H . In that case, can we tell whether there exists a sub-TeV Higgs boson or not? The answer is yes. It can be tested by carefully studying the scatterings of weak gauge bosons in the TeV region [10]. Furthermore, if the new physics causes a rather small HVV coupling (much below the value

of the SM HVV coupling), the production rate of a light Higgs boson can become so small that it escapes the detection when the experimental measurement is taken around the Higgs boson mass scale. However, as mentioned above, the scattering of $V_L V_L$ has to become large in the TeV region accordingly. Therefore, this makes it important to study the $V_L V_L$ scattering in the TeV regime even in the case where a light Higgs boson exists in the EWSB sector. We show in Sec. IV that this type of test of the anomalous HVV couplings is more sensitive than those obtained from Higgs boson production and decays [4–6], and may be more sensitive than the constraints from the precision electroweak data and the requirement of the unitarity of the S -matrix. Therefore, *studying the $V_L V_L$ scatterings at the LHC is not only important for probing the strongly interacting electroweak symmetry breaking sector without a light Higgs boson [9], but also valuable for sensitively testing of the anomalous gauge interactions of the Higgs boson when a light Higgs scalar exists in the mass range 115 – 300 GeV.* This further supports the “no-lose” theorem [9] for the LHC to decisively probe the EWSB mechanism.

This paper is organized as follows. In Sec. II, we briefly sketch the key points of studying VV scatterings related to the calculations in this paper. In Sec. III, we systematically study the test of the anomalous HVV coupling from the dimension-3 operator in a nonlinearly realized Higgs sector [11], as an extension of [7]. The test of the anomalous HVV couplings from the dimension-6 operators in the linearly realized Higgs sector [12,13] is studied in Sec. IV. In both cases, the constraints on the anomalous HVV couplings from the precision electroweak data and the requirement of the unitarity of the S -matrix are discussed. Sec. V summarize our concluding remarks.

II. VV SCATTERINGS

As mentioned in the previous section, we will take the enhanced VV scatterings as the signals for testing the anomalous HVV couplings. At the LHC, the initial state V 's in the VV scattering are emitted by the quarks in the protons. The transverse component V_T of the initial V can be greatly suppressed by tagging a forward-going jet (the out-going quark after emitting the V) [14,15], and thus the initial state V is essentially V_L by tagging the forward jet.

In this paper, we shall calculate the complete tree level contributions to the processes

$$pp \rightarrow VVjj, \quad (1)$$

where j is the forward jet. We will use the updated

CTEQ6L [16] parton distribution functions for the distributions of quarks in the protons, and take into account the width effect of the V -boson in the calculation of the helicity amplitudes.

We choose the gold-plated pure leptonic decay modes of the final state weak bosons as the tagging modes, this will avoid the large hadronic backgrounds at the LHC. Even in this case, there are still several kinds of backgrounds to be eliminated, namely the *electroweak (EW) background*, the *QCD background*, and the *top quark background* studied in Ref. [14,15]. Following Ref. [14,15], we impose, in addition to *forward jet tagging*, the requirements of *vetoing the central jet* to suppress the QCD background and the top quark background. The EW background can be suppressed by further *detecting isolated leptons with high P_T in the central rapidity region*, especially requiring the two final state leptons to be nearly back to back. These leptonic cuts also suppress the V_T contributions in the final state. Furthermore, choosing the decay leptons in the central rapidity region also avoids the collinear divergence in the diagrams exchanging a photon in $T(V, \gamma)$.

Ref. [17] studied various strongly interacting models which do not consist of a light Higgs boson and the $V_L V_L \rightarrow V_L V_L$ scattering amplitudes are largely enhanced (by powers of E^2) in the high energy region. The signal amplitudes were calculated in the effective W approximation (EWA) [18] because the $V_L V_L \rightarrow V_L V_L$ scattering amplitudes predicted by those models violate the unitarity condition of a $2 \rightarrow 2$ scattering matrix so that a full $2 \rightarrow 4$ process $pp \rightarrow V_L V_L jj$ could not be reliably calculated to predict the signal event rates in the TeV region. Instead, the $V_L V_L \rightarrow V_L V_L$ scattering amplitudes were properly unitarized before they were convoluted with the W -boson luminosities obtained from the EWA to predict the signal event rates. With this method of calculation, it was shown that after imposing the kinematic requirements discussed above, the backgrounds are reasonably suppressed relative to the signals, so that the $V_L V_L$ scatterings signals can be effectively extracted.

As to be discussed in Secs. III and VI, in our present case, the Higgs boson is light, and new physics effect is assumed to only modify the effective operators from a nonlinearly realized Higgs sector or a linearly realized Higgs sector. In the nonlinearly realized case, the $V_L V_L$ scattering amplitudes with a not too small anomalous HVV couplings are also enhanced in the high energy region due to the E^2 behavior of the amplitudes. Hence, we may apply the same methodology as proposed in Ref. [17] for calculating the signal rate. However, in this work, we choose not to use the EWA, instead, we compute the full $pp \rightarrow VVjj$ cross sections

at the tree level, cf. Eq. (1), which is justified as long as the LHC sensitivity to the size of the anomalous HVV coupling is below what required by the unitarity of the partial wave amplitudes of $V_L V_L \rightarrow V_L V_L$. As to be shown in Secs. III and IV, this is indeed the case and the backgrounds can be reasonably suppressed relative to the signals by imposing the same kinematical cuts suggested in Ref. [17]. On the contrary, in the case of the SM (without anomalous HVV couplings), all the $V_L V_L$, $V_T V_L$, and $V_T V_T$ amplitudes behave as E^0 rather than E^2 . Because the probability of finding a transverse vector boson (V_T) with high momentum is much larger than a longitudinal vector boson (V_L) [18], the contribution of $V_L V_L \rightarrow V_L V_L$ to the production rate of $pp \rightarrow VVjj$ in the TeV region is small as compared to the $V_T V_L$ and $V_T V_T$ contributions. Therefore, although the imposed kinematical cuts can effectively suppress the QCD and the top quark backgrounds, they leave a considerable EW background (mainly originated from the $V_T V_L$ and $V_T V_T$ contributions) that dominates the VV scattering in the SM. Throughout this paper, we will call these VV scattering contributions the remaining SM electroweak backgrounds after imposing the kinematical cuts. We note that since we will do the complete tree-level calculation for both the signal and the background processes by using the updated parton distribution functions and including the effect of the V boson width but without using the effective W approximation [18], even for the SM case, our results are not exactly the same as those given in Ref. [17].

In the case of a linearly realized effective Lagrangian, the physics consideration is quite different. As to be shown in Sec. VI, the $V_L V_L \rightarrow V_L V_L$ scattering amplitudes can have not only the E^2 but also the E^4 contributions depending on each process and operator under consideration. Furthermore, both the $V_T V_T \rightarrow V_L V_L$ and $V_L V_T \rightarrow V_L V_T$ scattering amplitudes can also have the E^2 contributions, which should be undoubtedly counted as part of the *signal* rates because those contributions are absent in the SM. Because the luminosity of V_T is larger than the V_L , the contributions from $V_T V_T$ and $V_T V_L$ scatterings cannot be ignored unless the E^4 contributions dominate the E^2 contributions which occur only when both the energy E and the anomalous couplings become large. It implies that the methodology used in Ref. [17] is not adequate in this case, and a full $2 \rightarrow 4$ calculation should be used to calculate the signal rates. Although it is possible to apply the EWA to include also the $V_T V_T$ and $V_L V_T$ contributions [19], with jet tagging efficiencies (for V_L and V_T , separately) extracted from the study done in Ref. [17], we choose to perform a full $pp \rightarrow VVjj$ tree-level calculation. This is justified as long as the anomalous

couplings are small so that the unitarity bounds are satisfied. Nevertheless, as to be discussed later, we will apply the EWA, folded with the $VV \rightarrow VV$ scattering amplitudes, to check the high energy behavior of the amplitudes from our full calculations which are also verified to be gauge invariant.

III. TESTING ANOMALOUS HVV COUPLING FROM DIMENSION-3 OPERATOR

A. The Anomalous HVV Coupling from Dimension-3 Operator

It is known that there is no anomalous HVV coupling arising from the dimension-3 and dimension-4 operators in the linearly realized effective Lagrangian [12,13]. Here, we consider the nonlinearly realized Higgs sector formulated in Ref. [11]. In this nonlinear formalism, the effective Lagrangian below the cutoff Λ contains the Higgs field H^0 transforming as a weak singlet, the would-be Goldstone boson field $\vec{\omega}$, and the electroweak gauge boson fields, and it respects the electroweak gauge symmetry, charge conjugation \mathbf{C} and parity \mathbf{P} , and the custodial $SU(2)_c$ symmetry. Up to dimension-4, the effective Lagrangian is given by [11]

$$\begin{aligned} \mathcal{L} = & -\frac{1}{4}\vec{W}_{\mu\nu} \cdot \vec{W}^{\mu\nu} - \frac{1}{4}B_{\mu\nu}B^{\mu\nu} \\ & + \frac{1}{4}(v^2 + 2\kappa v H + \kappa' H^2)\text{Tr}(D_\mu \Sigma^\dagger D^\mu \Sigma) \\ & + \frac{1}{2}\partial_\mu H \partial^\mu H - \frac{m_H^2}{2}H^2 - \frac{\lambda_3 v}{3!}H^3 + \frac{\lambda_4}{4!}H^4, \quad (2) \end{aligned}$$

where $\vec{W}_{\mu\nu}$ and $B_{\mu\nu}$ are field strengths of the electroweak gauge fields, $v \simeq 246 \text{ GeV}$ is the vacuum expectation value breaking the electroweak gauge symmetry, (κ, λ_3) and (κ', λ_4) are dimensionless coupling constants from the the dimension-3 and dimension-4 operators, respectively. In Eq. (2), we have defined

$$\begin{aligned} \Sigma = & \exp\left(\frac{i\vec{\tau} \cdot \vec{\omega}}{v}\right), \\ D_\mu \Sigma = & \partial_\mu \Sigma + ig\frac{\vec{\tau}}{2} \cdot \vec{W}_\mu \Sigma - ig'B_\mu \Sigma \frac{\tau_3}{2}, \quad (3) \end{aligned}$$

in which the Pauli matrix τ_i is normalized as $\text{Tr}(\tau_i \tau_j) = 2\delta_{ij}$, and g and g' are the $SU(2)_W$ and $U(1)_Y$ gauge coupling constants, respectively. The SM corresponds to $\kappa = \kappa' = 1$ and $\lambda_3 = \lambda_4 = \lambda = 3m_H^2/v^2$.

We note that at the tree level, only the dimension-3 operator $\frac{1}{2}\kappa v H D_\mu \Sigma^\dagger D^\mu \Sigma$ in Eq. (2) contains the anomalous HVV coupling that can contribute to the $V_L V_L$ scatterings (cf. Fig. 1). Therefore, the $V_L V_L$

scatterings can test this dimensionless coupling κ and $\Delta\kappa \equiv \kappa - 1$ measures the deviation from the SM value $\kappa = 1$.

B. Precision Constraints on the Coupling κ

The Eq. (2) shows an important difference between the nonlinearly and the linearly realized Higgs sectors. The nonlinear formalism allows new physics to appear in the effective operators with dimension ≤ 4 whose coefficients are not necessarily suppressed by the cutoff scale Λ . Hence, the gauge couplings of Higgs boson to weak bosons can naturally deviate from the SM-values by an amount at the order of $\lesssim \mathcal{O}(1)$, as suggested by the naive dimensional analysis [20].

In the unitary gauge, the relevant anomalous HVV couplings to the precision oblique parameters (S, T, U) [21] take the following form:

$$[(\kappa - 1)2vH + (\kappa' - 1)H^2] \left[\frac{2m_W^2}{v^2} W_\mu^+ W^{-\mu} + \frac{m_Z^2}{v^2} Z_\mu Z^\mu \right].$$

When calculating radiative corrections using the effective Lagrangian (2), it is generally necessary to introduce higher dimensional counter terms to absorb new divergences arising from the loop integration. There are in principle three next-to-leading order (NLO) counter terms to render the (S, T, U) parameters finite at the one-loop level,

$$\begin{aligned} \mathcal{L}^{(2')} = & \ell_0 \frac{v^2}{16\pi^2} \frac{1}{4} [\text{Tr} \mathcal{T} (D_\mu \Sigma) \Sigma^\dagger]^2, \\ \mathcal{L}_1^{(4)} = & \ell_1 \frac{v^2}{\Lambda^2} g g' \text{Tr} [\mathbf{B}_{\mu\nu} \Sigma^\dagger \mathbf{W}^{\mu\nu} \Sigma], \quad (4) \\ \mathcal{L}_8^{(4)} = & \ell_8 \frac{v^2}{\Lambda^2} \frac{g^2}{4} [\text{Tr} (\mathcal{T} \mathbf{W}_{\mu\nu})]^2, \end{aligned}$$

whose coefficients (ℓ_0, ℓ_1, ℓ_8) correspond to the oblique parameters (T, S, U) , respectively. Here $\mathbf{W}_{\mu\nu} = \vec{W}_{\mu\nu} \cdot \vec{\tau}/2$, $\mathbf{B}_{\mu\nu} = B_{\mu\nu} \tau_3/2$, and $\mathcal{T} \equiv \Sigma \tau_3 \Sigma^\dagger$. Comparing to $\mathcal{L}_1^{(4)}$, we note that $\mathcal{L}_8^{(4)}$ has the same dimension, but contains two new $SU(2)_c$ -violating operators \mathcal{T} , so that we expect $\ell_8/\ell_1 \sim 1/16\pi^2 \sim 10^{-2} \ll 1$. This generally leads to $U \ll S, T$. To estimate the contribution of loop corrections, we invoke a naturalness assumption that no fine-tuned accidental cancellation occurs between the leading logarithmic term and the constant piece of the counter terms. Thus, the leading logarithmic term represents a reasonable estimate of the loop corrections. This approach is commonly used in the literature for estimating new physics effects in effective theories [23]. It is straightforward to compute the radiative corrections to (S, T, U) due to the HVV

anomalous couplings, under the $\overline{\text{MS}}$ scheme, using dimensional regularization and keeping only the leading logarithmic terms. After subtracting the SM Higgs contributions ($\kappa = 1$) at the reference point m_H^{ref} , we find

$$\begin{aligned}\Delta S &= \frac{1}{6\pi} \left[\ln \frac{m_H}{m_H^{\text{ref}}} - (\kappa^2 - 1) \ln \frac{\Lambda}{m_H} \right] \\ \Delta T &= \frac{3}{8\pi c_w^2} \left[-\ln \frac{m_H}{m_H^{\text{ref}}} + (\kappa^2 - 1) \ln \frac{\Lambda}{m_H} \right], \\ \Delta U &= 0,\end{aligned}\tag{5}$$

where the $\ln \Lambda$ term represents the genuine new physics effect arising from physics above the cut-off scale Λ [24]. Note that at the one-loop order, the coupling κ' has no contribution to the S , T and U parameters. For a SM Higgs boson ($\kappa = 1$), a heavier Higgs mass will increase ΔS and decrease ΔT . Choosing the reference Higgs mass m_H^{ref} to be m_H , we may further simplify Eq. (5) as

$$\begin{aligned}\Delta S &= -\frac{\kappa^2 - 1}{6\pi} \ln \frac{\Lambda}{m_H}, \\ \Delta T &= +\frac{3(\kappa^2 - 1)}{8\pi c_w^2} \ln \frac{\Lambda}{m_H}, \\ \Delta U &= 0.\end{aligned}\tag{6}$$

For a given value of Λ and m_H , when $|\kappa| > 1$, we have $\Delta S < 0$ and $\Delta T > 0$. This pattern of radiative corrections allows a relatively heavy Higgs boson to be consistent with the current precision data [cf. Fig. 2(a)]. Furthermore, from Eq. (6) we see that the loop contribution from $\kappa \neq 1$ result in a sizable ratio of $\Delta T/\Delta S = -9/(4c_w^2) \approx -3$.

If we could *assume* no new physics beyond the SM, a global fit to the current precision electroweak data would suggest the SM Higgs boson to be light, with a central value $m_H = 83 \text{ GeV}$ (significantly below the LEP2 direct search limit $m_H > 114.3 \text{ GeV}$ [25]) and a 95% C.L. limit on the range of Higgs boson mass: $32 \text{ GeV} \leq m_H \leq 192 \text{ GeV}$. However, it was recently shown that in the presence of *new physics*, such a bound can be substantially relaxed [26–30]. We did not include the latest NuTeV data in the above fit. If we include the NuTeV data, the value of the minimum χ^2 of the global fit increases substantially (by 8.7), showing a poor quality of the SM fit to the precision data. (This fit also gives a similar central value, $m_H = 85 \text{ GeV}$, and 95% C.L. mass range $33 \text{ GeV} \leq m_H \leq 200 \text{ GeV}$.) We find a similar increase of χ^2 (by 8.9) also in the $\Delta S - \Delta T$ fits, suggesting that the NuTeV anomaly could not be explained by the new physics effect arising from the oblique parameters (ΔS , ΔT) alone. As the potential problems with

the NuTeV analysis are still under debate [31], we will not include the NuTeV data in the following analysis. [But for comparison, we have also displayed, in Fig. 2(a), a 95% C.L. contour (dotted curve) from the fit including the NuTeV anomaly.] In Fig. 2(a), we show the $\Delta S - \Delta T$ bounds (setting $m_H^{\text{ref}} = 100 \text{ GeV}$), derived from the global fits with the newest updated electroweak precision data [32,33]. Furthermore, for $m_H^{\text{ref}} = 115 (300) \text{ GeV}$ and $\Delta U = 0$, we find that the global fits give

$$\begin{aligned}\Delta S &= 0.01 (-0.07) \pm 0.09, \\ \Delta T &= 0.07 (0.16) \pm 0.11.\end{aligned}\tag{7}$$

In the same figure we also plot the contributions to ΔS and ΔT from the SM Higgs boson with different masses. Fig. 2(b) shows that the upcoming measurements of the W^\pm mass (m_W) and top mass (m_t) at the Tevatron Run-2 can significantly improve the constraints on new physics via the oblique corrections, where we input the errors of (m_W, m_t) to be the planned Run-2 sensitivity of 20 MeV and 2 GeV, respectively, and assumed the current Run-1 central values of (m_W, m_t) .

Using the allowed range of $(\Delta S, \Delta T)$ in Fig. 2(a), we can further constrain the new physics scale Λ as a function of the anomalous coupling $\Delta\kappa$ for a typical $m_H^{\text{ref}} = m_H$ value [cf. Eq. (6)]. The Fig. 3 depicts these constraints. With Fig. 3, we can alternatively constrain the range of $\Delta\kappa$ for a given value of (Λ, m_H) , which is summarized in Table I. Fig. 3 and Table I show that for $m_H \gtrsim 250 - 300 \text{ GeV}$, the $\Delta\kappa < 0$ region is fully excluded, while a sizable $\Delta\kappa > 0$ is allowed so long as Λ is relatively low. Moreover, for $m_H \gtrsim 800 \text{ GeV}$, the region $\Lambda < 1.1 \text{ TeV}$ is excluded. For $m_H \gtrsim 250 - 300 \text{ GeV}$ mass range, the preferred values of $\Delta\kappa > 0$ require the couplings of HW^+W^- and HZZ to be stronger than that of the SM, so that the direct production rate of the Higgs boson, via either the Higgs-strahlung or the VV fusions in high energy collisions, should raise above the SM rate. On the other hand, for $m_H \lesssim 250 \text{ GeV}$, the direct production rate of the Higgs boson can be smaller or larger than the SM rate depending on the sign of $\Delta\kappa$. Hence, when $\Delta\kappa < 0$, a light non-standard Higgs boson may be partially *hidden* by its large SM background events. However, in this situation, the new physics scale Λ will be generally low. For instance, when $m_H = 115 \text{ GeV}$, a negative $\Delta\kappa = -0.15 (-0.28)$ already forces $\Lambda \leq 1 (0.4) \text{ TeV}$. Finally, we mention that for certain class of models, new physics effects may also be induced by extra heavy fermions such as in the typical top-seesaw models with new vector-like fermions [26,34] or models with new chiral families [28]. In these models, there can be generic positive con-

tributions to ΔT , so that the $\Delta\kappa < 0$ region may still be allowed for a relatively heavy Higgs boson, but such possibilities are very model-dependent. In our current effective theory analysis, we consider the bosonic HVV couplings as the dominant contributions to the oblique parameters, and assume that other possible anomalous couplings (such as the deviation in the gauge interactions of $tbW/t\bar{t}Z$ [35]) can be ignored. However, independent of these assumptions, the *most decisive test* of the HVV couplings can come from the direct measurements via Born-level processes at the high energy colliders, which is the subject of the next two sections.

C. Constraints on κ from Unitarity Requirement

Before concluding this section, we discuss the possible unitarity violation in the scattering process $pp \rightarrow W^+W^+jj \rightarrow \ell\nu\ell\nu jj$ (for $\kappa \neq 1$), whose leading contribution comes from the sub-process $W_L^+W_L^+ \rightarrow W_L^+W_L^+$ when the initial W_L^+ bosons are almost collinearly radiated from the incoming quarks or antiquarks. The scattering amplitude of $W_L^+W_L^+ \rightarrow W_L^+W_L^+$ contributes to the isospin $I = 2$ channel, and in the high energy region ($E^2 \gg M_W^2, m_H^2$), is dominated by the leading E^2 -contributions,

$$T[I = 2] \simeq (\kappa^2 - 1) \frac{E^2}{v^2}. \quad (8)$$

Using the partial-wave analysis, its s -wave amplitude $a_{I,J=2,0}$ is derived as

$$a_{20} \simeq (\kappa^2 - 1) \frac{E^2}{16\pi v^2}, \quad (9)$$

where E ($= M_{VV}$) is the invariant mass of the vector boson pair. The unitarity condition for this channel is¹, $|\text{Re } a_{20}| < 2!/2 = 1$, and the factor $2!$ is due to the identical W^+W^+ in the final state. This results in a requirement,

$$\sqrt{1 - \frac{16\pi v^2}{E^2}} < |\kappa| < \sqrt{1 + \frac{16\pi v^2}{E^2}}. \quad (10)$$

For instance, it constrains

$$\begin{aligned} |\kappa| < 3.6, & \quad \text{for } E = 0.5 \text{ TeV}, \\ 0.5 < |\kappa| < 1.3, & \quad \text{for } E = 2 \text{ TeV}, \\ 0.8 < |\kappa| < 1.2, & \quad \text{for } E = 3 \text{ TeV}. \end{aligned} \quad (11)$$

¹Another convention in the literature [14,17] reads, $|\text{Re } a_{20}| < 1/2$, for $a_{20} \simeq (\kappa^2 - 1)E^2/(32\pi v^2)$. In this convention, the partial wave amplitude of the elastic scattering $W^+W^+ \rightarrow W^+W^+$, beyond the tree level, satisfies the relation $\text{Im } a = |a|^2$.

As to be shown in the next section, the expected sensitivity of the LHC to determining $\Delta\kappa$ [cf. Eq. (13)] is mainly consistent with the unitarity limit since the typical invariant mass of the W^+W^+ pair, after the kinematic cuts, falls into the range $500 \text{ GeV} \leq E \leq 2 \sim 3 \text{ TeV}$. The contributions from higher invariant mass values are severely suppressed by parton luminosities [17,36] and thus negligible.

IV. TESTING κ VIA VV SCATTERINGS AT THE LHC

Knowing the above constraints, we turn to the analysis of testing κ via VV scatterings at the LHC. Following the procedures described in Sec. II, we calculate the tree-level cross sections of the scattering processes

$$\begin{aligned} pp &\rightarrow Z_L Z_L jj \rightarrow \ell^+ \ell^- \ell^+ \ell^- jj, \ell^+ \ell^- \nu jj, \\ pp &\rightarrow W_L^+ W_L^- jj \rightarrow \ell^+ \nu \ell^- \bar{\nu} jj, \\ pp &\rightarrow W_L^+ W_L^+ jj \rightarrow \ell^+ \nu \ell^+ \nu jj, \\ pp &\rightarrow W_L^- W_L^- jj \rightarrow \ell^- \bar{\nu} \ell^- \bar{\nu} jj, \\ pp &\rightarrow Z_L W_L^+ jj \rightarrow \ell^+ \ell^- \ell^+ \nu jj, \\ pp &\rightarrow Z_L W_L^- jj \rightarrow \ell^+ \ell^- \ell^- \bar{\nu} jj. \end{aligned} \quad (12)$$

We have studied the contributions from different polarizations of W^+ and all the backgrounds discussed in Sec. III for $115 \text{ GeV} \leq m_H \leq 300 \text{ GeV}$. The contributions of different polarizations of W^+W^+ to the cross section in the W^+W^+ channel for $m_H = 115 \text{ GeV}$ and various values of $\Delta\kappa$ are listed in Table II. As expected, when $|\Delta\kappa|$ is large, the $W_L^+W_L^+$ rate dominates over the other polarization states of the W bosons. We also find that all the SM backgrounds are reasonably suppressed relative to the signal by the kinematical cuts for the case of $\Delta\kappa$ significantly different from 0, for the E^2 -dependence of the $W_L W_L$ amplitude enhances the signal rate. However, for $\Delta\kappa = 0$ (the SM), only the QCD and top quark backgrounds are negligibly small, while the EW background contributed from the TT and LT polarizations are still quite large as compared to the signal. Therefore, in this work, we will take the cross section for $\Delta\kappa = 0$ (the SM) as the remained background cross section after imposing the relevant kinematic cuts to enhance the signal of longitudinal weak boson scatterings.

In Tables III–VI, we list the obtained numbers of events (including both the signals and backgrounds) for an integrated luminosity of 300 fb^{-1} with the parameters $115 \text{ GeV} \leq m_H \leq 300 \text{ GeV}$ and $-1.0 \leq$

$\Delta\kappa \leq 0.7^2$. We see that the most sensitive channel to determine the anomalous coupling $\Delta\kappa$ is $pp \rightarrow W^+W^+jj \rightarrow l^+\nu l^+\nu jj$ (cf. Table III) due to its small background rates, and thus the weakest kinematic cuts [17].

It is easy to check that the numbers in Tables V and VI, for the ZW^\pm and ZZ channels, are mainly consistent with the unitarity bound. Only the W^+W^- channel, cf. Table IV, needs further unitarization [17]. It is expected that after unitarizing the scattering amplitudes, the corresponding numbers in Table IV will become smaller, and thus this channel is less interesting. Therefore, in this paper we only take the best channel, the W^+W^+ channel (cf. Table III), to constrain $\delta\kappa$.

As discussed in Sec. II, we will take the 15 – 16 SM events (for $\Delta\kappa = 0$) listed in Table III as the intrinsic SM electroweak background rates after imposing the kinematical cuts, i.e. $N_B \equiv N(\Delta\kappa = 0)$. We can then define the signal events for $\Delta\kappa \neq 0$ as $N_S \equiv N(\Delta\kappa \neq 0) - N_B$. The total statistical fluctuation is $\sqrt{N_S + N_B}$. To see the potential of the LHC in distinguishing the $\Delta\kappa \neq 0$ case from the SM, we also show the deviation of the signal from the total statistical fluctuation, $N_S/\sqrt{N_S + N_B}$, in the parentheses in Tables III and IV. The values of $N_S/\sqrt{N_S + N_B}$ in Table III show that the LHC can limit $\Delta\kappa$ to the range

$$-0.3 < \Delta\kappa < 0.2 \quad (13)$$

at roughly $(1 - 3)\sigma$ level if no anomalous coupling ($\Delta\kappa \neq 0$) effect is detected.

As mentioned in Sec. I, if the new physics above the cutoff scale Λ happens to make $\Delta\kappa$ negative and close to $\Delta\kappa = -1$ ($\kappa \gtrsim 0$), the Higgs production rate may become so small that the Higgs resonance may be hard to detect. However, we see from Table III that the event numbers of $pp \rightarrow W^+W^+jj \rightarrow l^+\nu l^+\nu jj$ for this κ value are much larger than those for the SM, so that we can clearly detect the $\kappa \gtrsim 0$ effect via these processes without the need of detecting the resonance of a light Higgs boson. This is the clear advantage of such type of measurements when the resonant state of the Higgs boson is difficult to be detected experimentally.

²In principle, the number of events for $\kappa > 0$ and $\kappa < 0$ are not the same. However, our obtained results show that the difference between them is very small. So only list the number of events with $\Delta\kappa \geq -1$ ($\kappa \geq 0$) in the Tables.

V. OTHER POSSIBLE TESTS OF κ FROM FUTURE COLLIDER EXPERIMENTS

There can be other possible tests of κ from future collider experiments. We discuss them below in order.

A. Associate HV Production

The first one is from the associated production of Higgs boson and vector boson ($H + V$) productions at high energy colliders. The studies at LEP-2 concluded that the mass of the SM Higgs boson has to be larger than about 114.3 GeV [25]. For a non-SM Higgs boson, this lower mass bound will be different. For example, in the supersymmetric SM, the H - Z - Z coupling is smaller than that of the SM by a factor $\sin(\alpha - \beta)$ or $\cos(\alpha - \beta)$, depending whether H denotes a light or a heavy CP-even Higgs boson, and this lower mass bound is reduced to about 90 GeV [37]. If the mass of the SM Higgs boson is around 110 GeV, it can be discovered at the Tevatron Run-2. Assuming an integrated luminosity of 10 fb^{-1} , the number of the expected signal events is about 27 and the background events about 258, according to the Table 3 (the most optimal scenario) of Ref. [38]. Therefore, the one sigma statistic fluctuation of the total event is $\sqrt{27 + 258} \sim 17$. Consequently, at the 1σ level, $0.6 < |\kappa| < 1.2$, and at the 2σ level, $|\kappa| < 1.5$.³ Similarly, we estimate the bounds on $|\kappa|$ for various m_H as follows:

$m_H(\text{GeV})$	1σ	2σ
110 :	$0.6 \leq \kappa \leq 1.2,$	$0 \leq \kappa \leq 1.5,$
120 :	$0.4 \leq \kappa \leq 1.4,$	$0 \leq \kappa \leq 1.6,$
130 :	$0 \leq \kappa \leq 1.5,$	$0 \leq \kappa \leq 1.8,$

(14)

We see that the above limits on κ are weaker than that in Eq. (13). Of course, the above bounds can be further improved at the Tevatron Run-2 by having a larger integrated luminosity until the systematical error dominates the statistical error. The same process can also be studied at the LHC to test the anomalous coupling κ . However, because of the much larger background rates at the LHC, the improvement on the measurement of κ via the associated production of V and Higgs boson is not expected to be significant.

³This bound can be improved by carefully examining the invariant mass distribution of the $b\bar{b}$ pairs.

B. Measuring Total Decay Width of Higgs Boson

Another possible test is from the expected precision of measuring the total width of the Higgs boson. When the Higgs boson mass is larger than twice of the Z boson mass, it can decay into a Z boson pair which subsequently decay into 4 muons. This decay channel is labelled as one of the “gold-plated” channels (the pure leptonic decay modes) because it is possible to construct the invariant mass of the ZZ pair in this decay mode with a high precision, which provides a precision measurement on the total decay width of the Higgs boson. A detailed Monte Carlo analysis has been carried out in Ref. [39] to find out the uncertainty on the measurement of the Higgs boson width. Assuming that there is no non-SM decay channel opened and only the anomalous HVV coupling is important, one can convert the conclusion from [39] to the bounds on $\Delta\kappa$. Since the decay branching ratio of $H \rightarrow W^+W^-$ or ZZ for a SM heavy Higgs boson is large (almost one hundred percent for $m_H > 300\text{ GeV}$), the total width measurement can give a strong constraint on κ . From the Table 3 of Ref. [39], we define the accuracy on the determination of κ using the relation $-n\Delta\Gamma \leq \Gamma(\kappa) - \Gamma(\kappa = 1) \leq n\Delta\Gamma$, where $n = 1, 2$ denoting the 1σ and 2σ accuracy, respectively, and $\Gamma(\kappa)$ is the width of the Higgs boson for a general value of κ , $\Gamma(\kappa = 1)$ is for a SM Higgs boson and $\Delta\Gamma$ is the experimental accuracy in measuring the Higgs boson width. We find that at the LHC (with an integrated luminosity of 300 fb^{-1} [40]), the bounds on $\Delta\kappa$ obtained from the measurement of the total decay width of Higgs boson, via the process $pp \rightarrow H \rightarrow ZZ \rightarrow \mu^+\mu^-\mu^+\mu^-$ are

$m_H(\text{GeV})$	1σ	2σ
200 – 300 :	$0.9 \leq \kappa \leq 1.1,$	$0.8 \leq \kappa \leq 1.2.$

(15)

C. Decay Branching Ratio of $H \rightarrow \gamma\gamma$

Another important effect of a non-vanishing anomalous coupling κ is to change the decay branching ratio of $H \rightarrow \gamma\gamma$, which determines the production rate of $gg \rightarrow H \rightarrow \gamma\gamma$ at the LHC. In Table VII, we list the decay branching ratio $B(H \rightarrow \gamma\gamma)$ as a function of κ for various m_H . As shown, $B(H \rightarrow \gamma\gamma)$ decreases for $\kappa > 1$, and increases for $\kappa < 1$.

D. Detecting a Higgs Boson Resonance

When the SM Higgs boson is light, it is expected that the production rate of $qq \rightarrow qqH$ with $H \rightarrow$

$WW^* \rightarrow \ell\ell'\bar{\nu}_T$ is large enough to be detected at the LHC, and this process can also be used to test the coupling of the HWW [41] by studying the observables near the Higgs boson resonance. In the effective Lagrangian (2), the Lorentz structure (and the dimension) of the anomalous couplings κ and κ' is the same as the SM coupling. Therefore, the result of the study performed in Ref. [41] also holds for the current study when m_H is less than twice of the Z boson mass. In this case, its production rate is $\kappa^2\mathcal{S}_{SM}B(\kappa)/B(\kappa = 1)$, where \mathcal{S}_{SM} is the SM rate, and $B(\kappa)$ is the decay branching ratio of $H \rightarrow WW^*$ for a general value of κ . Needless to say that $B(\kappa = 1)$ corresponds to the SM branching ratio.

When the WW (and ZZ) decay mode dominates the Higgs boson decay, such as when m_H is larger than twice of W boson mass, the ratio of the decay branching ratios for $H \rightarrow WW^*$, $B(\kappa)/B(\kappa = 1)$, would be close to 1. However, this ratio can be quite different from 1 when m_H is small. For example, for $\kappa = 0.8$ and $\kappa = 1.2$, the ratio $B(\kappa)/B(\kappa = 1)$ is 0.65 and 1.4, respectively, for $m_H = 110\text{ GeV}$. Let \mathcal{B} be the background rate, and denote $\kappa^2B(\kappa)/B(\kappa = 1)$ as R . From the Table 1 of Ref. [41], one can determine the constraint on R using the relation $\mathcal{S}_{SM} - n\sqrt{\mathcal{B} + \mathcal{S}_{SM}} \leq R\mathcal{S}_{SM} \leq \mathcal{S}_{SM} + n\sqrt{\mathcal{B} + \mathcal{S}_{SM}}$, where $n = 1, 2$ denotes the 1σ and 2σ accuracy, respectively. Assuming an integrated luminosity of 300 fb^{-1} , we find that the bounds on R for various m_H are:

m_H (GeV)	1σ	2σ
110 :	$0.87 \leq R \leq 1.13,$	$0.74 \leq R \leq 1.26,$
120 :	$0.94 \leq R \leq 1.06,$	$0.88 \leq R \leq 1.12,$
130 :	$0.97 \leq R \leq 1.03,$	$0.93 \leq R \leq 1.07,$
150 :	$0.97 \leq R \leq 1.03,$	$0.94 \leq R \leq 1.06,$
170 :	$0.98 \leq R \leq 1.02,$	$0.95 \leq R \leq 1.05.$

(16)

To extract the bound on κ , we need to know the decay branching ratio $B(\kappa)$ of $H \rightarrow WW^*$ assuming that the effective Lagrangian (2) differs from the SM Lagrangian only in the coefficient κ . A few values of $B(\kappa)$ as a function of κ for various m_H are given in Table VIII. The result of Table VIII and Eq. (16) indicate that κ can be measured at a few percent level when a light Higgs boson is detected. However, in our opinion, this conclusion seems to be too optimistic because the systematical error of the experiment at the LHC is expected to be at least at the same level of accuracy.

Before closing this section, we note that the anomalous coupling of H - Z - Z can also be tested via the process $e^-e^+ \rightarrow ZH(\rightarrow b\bar{b})$ at the future Linear Collider. In Ref. [3], it was concluded that $\Delta\kappa$ can be determined at the percent level for a 120 GeV SM Higgs

boson associatedly produced with the Z boson at a 250 GeV e^-e^+ collider. Thus, the expected precision in the measurement of $\Delta\kappa$ at the LC is higher than that at the LHC, as given in Eq. (13). However, we shall show in the next section that the determination of the dimension-6 anomalous couplings via VV scatterings at the LHC will be of the similar level of precision as at the LC.

VI. TESTING ANOMALOUS HVV COUPLINGS FROM DIMENSION-6 OPERATORS

A. Anomalous HVV Couplings from Dimension-6 Operators

Now we consider the test of the anomalous HVV couplings from the dimension-6 operators arising from the linearly realized effective Lagrangian. In the linearly realized effective Lagrangian, there is no non-standard operators at dimension-3 and dimension-4, and leading anomalous HVV couplings are found to arise from effective operators of dimension-6. In the following, we will analyze the test of these leading order anomalous couplings. As is shown in Ref. [12,13], the C and P conserving effective Lagrangian up to dimension-6 operators, containing a Higgs doublet Φ and the weak bosons V^a , is given by

$$\mathcal{L}_{\text{eff}} = \sum_n \frac{f_n}{\Lambda^2} \mathcal{O}_n, \quad (17)$$

where f_n 's are anomalous coupling constants (the SM corresponds to $f_n = 0$). The operators \mathcal{O}_n 's are [13]

$$\begin{aligned} \mathcal{O}_{\Phi,1} &= (D_\mu \Phi)^\dagger \Phi^\dagger \Phi (D^\mu \Phi), \\ \mathcal{O}_{BW} &= \Phi^\dagger \hat{B}_{\mu\nu} \hat{W}^{\mu\nu} \Phi, \\ \mathcal{O}_{DW} &= \text{Tr} \left([D_\mu, \hat{W}_{\nu\rho}] [D^\mu, \hat{W}^{\nu\rho}] \right), \\ \mathcal{O}_{DB} &= -\frac{g'^2}{2} (\partial_\mu B_{\nu\rho}) (\partial^\mu B^{\nu\rho}), \\ \mathcal{O}_{\Phi,2} &= \frac{1}{2} \partial^\mu (\Phi^\dagger \Phi) \partial_\mu (\Phi^\dagger \Phi), \\ \mathcal{O}_{\Phi,3} &= \frac{1}{3} (\Phi^\dagger \Phi)^3, \\ \mathcal{O}_{WWW} &= \text{Tr} [\hat{W}_{\mu\nu} \hat{W}^{\nu\rho} \hat{W}_\rho^\mu], \\ \mathcal{O}_{WW} &= \Phi^\dagger \hat{W}_{\mu\nu} \hat{W}^{\mu\nu} \Phi, \\ \mathcal{O}_{BB} &= \Phi^\dagger \hat{B}_{\mu\nu} \hat{B}^{\mu\nu} \Phi, \\ \mathcal{O}_W &= (D_\mu \Phi)^\dagger \hat{W}^{\mu\nu} (D_\nu \Phi), \\ \mathcal{O}_B &= (D_\mu \Phi)^\dagger \hat{B}^{\mu\nu} (D_\nu \Phi), \end{aligned} \quad (18)$$

where $\hat{B}_{\mu\nu}$ and $\hat{W}_{\mu\nu}$ stand for

$$\hat{B}_{\mu\nu} = i\frac{g'}{2} B_{\mu\nu}, \quad \hat{W}_{\mu\nu} = i\frac{g}{2} \sigma^a W_{\mu\nu}^a. \quad (19)$$

At the tree level, the operators $\mathcal{O}_{\Phi,1}$, \mathcal{O}_{BW} , \mathcal{O}_{DW} and \mathcal{O}_{DB} in Eq. (18) affect the two-point functions of the weak boson V when Φ is taken to be its vacuum expectation value

$$\Phi \rightarrow \frac{1}{\sqrt{2}} \begin{pmatrix} 0 \\ v \end{pmatrix}. \quad (20)$$

The two operators $\mathcal{O}_{\Phi,2}$ and $\mathcal{O}_{\Phi,3}$ in Eq. (18) lead to a finite renormalization of the Higgs wave function and the Higgs potential [13]. The last five operators \mathcal{O}_{WWW} , \mathcal{O}_{WW} , \mathcal{O}_{BB} , \mathcal{O}_W and \mathcal{O}_B in Eq. (18) contribute to the three- and four-point functions of V and to the HVV couplings [12]. What we are interested in the present study are the operators \mathcal{O}_{WW} , \mathcal{O}_{BB} , \mathcal{O}_W and \mathcal{O}_B which lead to the following anomalous HVV couplings [13]

$$\begin{aligned} \mathcal{L}_{\text{eff}}^H &= g_{H\gamma\gamma} H A_{\mu\nu} A^{\mu\nu} + g_{HZ\gamma}^{(1)} A_{\mu\nu} Z^\mu \partial^\nu H \\ &+ g_{HZ\gamma}^{(2)} H A_{\mu\nu} Z^{\mu\nu} + g_{HZZ}^{(1)} Z_{\mu\nu} Z^\mu \partial^\nu H \\ &+ g_{HZZ}^{(2)} H Z_{\mu\nu} Z^{\mu\nu} + g_{HWW}^{(1)} (W_{\mu\nu}^+ W^{-\mu} \partial^\nu H + \text{h.c.}) \\ &+ g_{HWW}^{(2)} H W_{\mu\nu}^+ W^{-\mu\nu}, \end{aligned} \quad (21)$$

where

$$\begin{aligned} g_{H\gamma\gamma} &= -\left(\frac{gM_W}{\Lambda^2}\right) \frac{s^2(f_{BB} + f_{WW})}{2}, \\ g_{HZ\gamma}^{(1)} &= \left(\frac{gM_W}{\Lambda^2}\right) \frac{s(f_W - f_B)}{2c}, \\ g_{HZ\gamma}^{(2)} &= \left(\frac{gM_W}{\Lambda^2}\right) \frac{s[s^2 f_{BB} - c^2 f_{WW}]}{c}, \\ g_{HZZ}^{(1)} &= \left(\frac{gM_W}{\Lambda^2}\right) \frac{c^2 f_W + s^2 f_B}{2c^2}, \\ g_{HZZ}^{(2)} &= -\left(\frac{gM_W}{\Lambda^2}\right) \frac{s^4 f_{BB} + c^4 f_{WW}}{2c^2}, \\ g_{HWW}^{(1)} &= \left(\frac{gM_W}{\Lambda^2}\right) \frac{f_W}{2}, \\ g_{HWW}^{(2)} &= -\left(\frac{gM_W}{\Lambda^2}\right) f_{WW}, \end{aligned} \quad (22)$$

with $s \equiv \sin\theta_W$, $c \equiv \cos\theta_W$. In our calculation, we have included the complete gauge invariant set of Feynman diagrams that receive contribution from the anomalous operators \mathcal{O}_{WWW} , \mathcal{O}_{WW} , \mathcal{O}_{BB} , \mathcal{O}_W and \mathcal{O}_B .

In Eq. (21), the anomalous HVV couplings are expressed as effective form factors of the Lorentz-invariant (but not gauge-invariant) dimension-5 operators, which can all result from the gauge-invariant dimension-6 operators in the linear realizations [cf.

(22)]. A few of them can also be induced from the gauge-invariant dimension-5 operators in the nonlinear realization of the Higgs sector because in this scenario the Higgs field H is an electroweak singlet. Thus, it is worth to note that the following LHC study of testing the linearly realized anomalous HVV couplings via the VV scatterings may be readily generalized to the case of the dimension-5 operators in the nonlinear realization.

B. Constraints on f_n from the Existing Experiments and the Unitarity Requirement

There are known experiments that can constrain the size of the anomalous coupling constants f_n .

The constraints on the anomalous coupling constants f_{WWW} , f_{WW} , f_{BB} , f_W and f_B have been studied in Refs. [13,42,43]. At tree level, ΔS and ΔT are proportional to f_{BW}/Λ^2 and $f_{\Phi,1}/\Lambda^2$, respectively. Thus we can obtain the 68% and 95% CL bounds on the (f_{BW}/Λ^2) - $(f_{\Phi,1}/\Lambda^2)$ plane directly from the corresponding bounds in Fig. 2(a). This is shown in Fig. 4. We see from Fig. 4 that the precision data give quite strong constraints on f_{BW}/Λ^2 and $f_{\Phi,1}/\Lambda^2$. At one loop level, ΔS and ΔT are related to other five anomalous coupling constants through loop corrections. Following Refs. [13,42,43], we make a one parameter fit of the five anomalous coupling constants by using the formulas given in Ref. [43] and the updated ΔS - ΔT bounds in Fig. 2(a). The obtained 95% CL constraints (in units of TeV^{-2}) for $m_H = 100$ GeV are:

$$\begin{aligned} -6 &\leq f_{WWW}/\Lambda^2 \leq 3, \\ -6 &\leq f_W/\Lambda^2 \leq 5, \\ -4.2 &\leq f_B/\Lambda^2 \leq 2.0, \\ -5.0 &\leq f_{WW}/\Lambda^2 \leq 5.6, \\ -17 &\leq f_{BB}/\Lambda^2 \leq 20. \end{aligned} \quad (23)$$

These constraints are much weaker than that shown in Fig. 4 because these five anomalous coupling constants contribute to ΔS and ΔT through one loop corrections which are suppressed by the loop factor $1/16\pi^2$.

The triple gauge coupling data lead to the following 95% CL constraints (in units of TeV^{-2}) [4,13,44,45]:

$$\begin{aligned} -31 &\leq (f_W + f_B)/\Lambda^2 \leq 68 \quad \text{for } f_{WWW} = 0, \\ -41 &\leq f_{WWW}/\Lambda^2 \leq 26 \quad \text{for } f_W + f_B = 0. \end{aligned} \quad (24)$$

Furthermore, the Higgs searches data at LEP2 and Tevatron can give rise to the following 95% CL bound on $f_{WW(BB)}$ (in units of TeV^{-2}) for $m_H \leq 150$ GeV [4]

$$-7.5 \leq \frac{f_{WW(BB)}}{\Lambda^2} \leq 18. \quad (25)$$

The theoretical constraint on f_n coming from the requirement of the unitarity of the S -matrix has been studied in Ref. [46]. In terms of the present symbols of the anomalous coupling constants, the unitarity bounds given in Ref. [46] read (in units of TeV^{-2})

$$\left| \frac{f_B}{\Lambda^2} \right| \leq \frac{98}{\Lambda^2}, \quad \left| \frac{f_W}{\Lambda^2} \right| \leq \frac{31}{\Lambda^2},$$

$$-\frac{784}{\Lambda^2} + \frac{3556M_W}{\Lambda^3} \leq \frac{f_{BB}}{\Lambda^2} \leq \frac{638}{\Lambda^2} + \frac{3733M_W}{\Lambda^3},$$

$$\left| \frac{f_{WW}}{\Lambda^2} \right| \leq \frac{35.2}{\Lambda^2} + \frac{4.86}{\Lambda M_W}, \quad \left| \frac{f_{WWW}}{\Lambda^2} \right| \leq \frac{38}{3g^2\Lambda^2}, \quad (26)$$

in which we have put the center-of-mass energy $\sqrt{s} \approx \Lambda$. For $\Lambda \approx 2$ TeV, the bounds are (in units of TeV^{-2})

$$\left| \frac{f_B}{\Lambda^2} \right| \leq 24.5 \quad \left| \frac{f_W}{\Lambda^2} \right| \leq 7.8 \quad \left| \frac{f_{WWW}}{\Lambda^2} \right| \leq 7.5,$$

$$-160 \leq \frac{f_{BB}}{\Lambda^2} \leq 197, \quad \left| \frac{f_{WW}}{\Lambda^2} \right| \leq 39.2. \quad (27)$$

These bounds are essentially of the same level as the above bounds (23) and (24).

We see that except the constraints from the precision data (cf. Fig. 4), all the other constraints are rather weak. Furthermore, the above constraints on f_n/Λ^2 lead to the following constraints (in units of TeV^{-1}) on the anomalous coupling constants $g_{HWW}^{(1)}$, $g_{HWW}^{(2)}$, $g_{HZZ}^{(1)}$ and $g_{HZZ}^{(2)}$, that are related to the VV scatterings:

$$\begin{aligned} -0.20 &\leq g_{HWW}^{(1)} \leq 0.065, \\ -1.2 &\leq -g_{HWW}^{(2)} \leq 0.73, \\ -0.26 &\leq g_{HZZ}^{(1)} \leq 0.24, \\ -0.62 &\leq -g_{HZZ}^{(2)} \leq 0.36. \end{aligned} \quad (28)$$

We shall see in the following subsection that the limits on these coupling constants obtained from $V_L V_L$ scatterings at the LHC will be significantly stronger than Eq. (28).

C. Testing f_n via VV Scatterings at the LHC

The test of the anomalous HVV couplings from the dimension-6 operators via VV scatterings is quite different from that for the dimension-3 operator. The

relevant operators in Eq. (18) contain two derivatives, so that the interactions themselves behave as E^2 at high energies. Thus, at high energies, the scattering amplitudes of the longitudinal components V_L behave as E^4 , and those containing transverse components V_T behave at least as E^2 . We see that scatterings containing V_T actually behave as *signals* rather than backgrounds. This is very different from the case of the dim-4 anomalous coupling. As discussed in Sec. II, since the $V_T V_T$ and $V_L V_T$ scatterings also contribute to the signal rate, we decide to do the full $2 \rightarrow 4$ tree level calculation, in contrast to performing the calculation using the EWA folded by the $2 \rightarrow 2$ VV scattering amplitudes. Nevertheless, we shall use the EWA to check the high energy behavior of the full calculation when the anomalous coupling is large.

We calculate the tree level cross sections for all the processes listed in Eq. (12) with the same method described in Sec. II, but for the linearly realized effective Lagrangian theory. Since there are several dim-6 anomalous couplings related to the VV scatterings in this theory [cf. Eq. (18)], the analysis is more complicated than in the dim-4 case. If the anomalous coupling constants are of the same order of magnitude, the interferences between them may be significant, depending on the relative phases among them. This undoubtedly complicates the analysis. In the following, we follow the same methodology as in Eq. (23) and perform the single parameter analysis, i.e. assuming only one of the anomalous coupling constants is dominant at a time. We see from Eq.(18) that the coupling constants related to VV scatterings are f_{WWW} , f_{WW} , f_{BB} , f_W and f_B . f_{WWW} is the anomalous coupling of the triple gauge boson vertex which may not be directly related to the electroweak symmetry breaking mechanism, so we assume it is small in the analysis. Detailed calculations show that the contributions of f_B and f_{BB} to the most sensitive $pp \rightarrow W^+ W^+ jj \rightarrow W^+ W^+ l^+ \nu l^+ \nu jj$ channel are small even if they are of the same order of magnitude as other anomalous coupling constants. So we ignore f_B and f_{BB} in the analysis. Then there are mainly two anomalous coupling constants left, namely f_W and f_{WW} . We shall show the sensitivity of determining these two coupling constants via VV scatterings individually.

In the case that f_W dominates, the obtained numbers of events with an integrated luminosity 300 fb^{-1} for various values of m_H and f_W/Λ^2 are listed in Table IXA and Table X–Table XII. From these Tables, we see that the most sensitive channel is still $pp \rightarrow W^+ W^+ jj \rightarrow W^+ W^+ l^+ \nu l^+ \nu jj$, as listed in Table IXA. All other channels are less interesting. Similar to the numbers in Table III, the 15–16 events for $f_W/\Lambda^2 = 0$ (the SM case) are the SM backgrounds

after the cuts, i.e., $N_B = N(f_W = 0)$. The number of the signal events is defined as $N_S = N(f_W \neq 0) - N_B$. We also list the values of the deviation of the signal from the total statistical fluctuation, $N_S/\sqrt{N_S + N_B}$, in the parentheses in Table IXA and Table IXB. If no anomalous coupling effect is found via this process, we can set the following bounds for f_W/Λ^2 (in units of TeV^{-2}):

$$\begin{aligned} 1\sigma : & \quad -1.0 < f_W/\Lambda^2 < 0.85 \\ 2\sigma : & \quad -1.4 < f_W/\Lambda^2 \leq 1.2, \end{aligned} \quad (29)$$

roughly for all values of m_H in the range $115 \text{ GeV} \lesssim m_H \lesssim 300 \text{ GeV}$.

In the case that f_{WW} dominates, the corresponding numbers of events are listed in Table IXB. We see that the bounds are weaker, i.e. (in units of TeV^{-2}),

$$\begin{aligned} 1\sigma : & \quad -1.6 \leq f_{WW}/\Lambda^2 < 1.6, \\ 2\sigma : & \quad -2.2 \leq f_{WW}/\Lambda^2 < 2.2, \end{aligned} \quad (30)$$

To see the effect of interference, we take a special case as an example. We take $f_W = -f_{WW} \equiv f$, i.e., $g_{HVV}^{(1)}$ and $g_{HVV}^{(2)}$ in Eq. (22) are of the same sign. Then we get the following bounds (in units of TeV^{-2}):

$$\begin{aligned} 1\sigma : & \quad -0.6 \leq f/\Lambda^2 \leq 0.5, \\ 2\sigma : & \quad -0.9 \leq f/\Lambda^2 \leq 0.75. \end{aligned} \quad (31)$$

In this case, the interference enhances the sensitivity. Of course, if $f_W = f_{WW} = f$, the sensitivity will be reduced.

From the bounds in Eqs. (29)–(30), together with the relations in Eq. (22), we obtain the corresponding bounds on $g_{HVV}^{(i)}$, $i = 1, 2$ (in units of TeV^{-1}):

$$\begin{aligned} 1\sigma : & \\ & -0.026 < g_{HWW}^{(1)} < 0.022, \\ & -0.026 < g_{HZZ}^{(1)} < 0.022, \\ & -0.014 < g_{HZZ\gamma}^{(1)} < 0.012, \\ & -0.083 \leq g_{HWW}^{(2)} < 0.083, \\ & -0.032 \leq g_{HZZ}^{(2)} < 0.032, \\ & -0.018 \leq g_{HZZ\gamma}^{(2)} < 0.018, \\ 2\sigma : & \\ & -0.036 < g_{HWW}^{(1)} \leq 0.031, \\ & -0.036 < g_{HZZ}^{(1)} \leq 0.031, \\ & -0.020 < g_{HZZ\gamma}^{(1)} \leq 0.017, \\ & -0.11 \leq g_{HWW}^{(2)} < 0.11, \\ & -0.044 \leq g_{HZZ}^{(2)} < 0.044, \\ & -0.024 \leq g_{HZZ\gamma}^{(2)} < 0.024. \end{aligned} \quad (32)$$

These bounds are to be compared with the 1σ bound on $g_{HWW}^{(2)}$ obtained from studying the Higgs boson production via weak boson fusion at the LHC, as given recently in Ref. [6]. In Ref. [6], $g_{HWW}^{(2)}$ is parameterized as $g_{HWW}^{(2)} = 1/\Lambda_5 = g^2 v/\Lambda_6^2$, and the obtained 1σ bound on Λ_6 for an integrated luminosity of 100 fb^{-1} is about $\Lambda_6 \gtrsim 1 \text{ TeV}$, which corresponds to $g_{HWW}^{(2)} = 1/\Lambda_5 \leq 0.1 \text{ TeV}^{-1}$. We see that the 1σ bounds listed in Eq. (32) are all stronger than this bound. For an integrated luminosity of 300 fb^{-1} , the bound $g_{HWW}^{(2)} = 1/\Lambda_5 \leq 0.1 \text{ TeV}^{-1}$ given in Ref. [6] corresponds roughly to the 1.7σ level. Then we can roughly compare our 2σ bounds in Eq. (32) with it. We see that our 2σ bound of $g_{HWW}^{(2)}$ is about the same, while our 2σ bounds on the other five $g_{HVV}^{(i)}$ ($i = 1, 2$) are stronger than it.

It has been shown in Ref. [3] that the anomalous HZZ coupling constants $g_{HZZ}^{(1)}$ and $g_{HZZ}^{(2)}$ can be tested rather sensitively at the LC via the Higgs-strahlung process $e^+e^- \rightarrow Z^* \rightarrow Z+H$ and the decay mode $Z \rightarrow f\bar{f}$. In Ref. [3], $g_{HZZ}^{(1)}$ and $g_{HZZ}^{(2)}$ are parameterized as $g_{HZZ}^{(1)} = \frac{g_Z}{M_Z} c_V$ and $g_{HZZ}^{(2)} = \frac{g_Z}{M_Z} b_Z$, respectively. The obtained limits on the coefficients c_V and b_V are $c_V \sim b_V \sim O(10^{-3})$ [3] which corresponds to the limits $g_{HZZ}^{(1)} \sim g_{HZZ}^{(2)} \sim O(10^{-3}-10^{-2}) \text{ TeV}^{-1}$. Although the LHC W^+W^+ scattering bounds shown in Eq. (32) is weaker than these LC bounds, W^+W^+ scattering at the LHC provides the bounds on $g_{HWW}^{(i)}$, $i = 1, 2$. So that the two experiments are complementary to each other.

To verify that our calculation does give the correct asymptotic behavior as that given in Ref. [46], and to see the difference between the complete tree level result and the EWA result (with only the $V_L V_L \rightarrow V_L V_L$ contribution included), we plot in Fig. 5 the M_{WW} distributions in the W^+W^+ channel with $f_W/\Lambda^2 = 5 \text{ TeV}^{-2}$ from the complete tree level result (solid line), the EWA result with only the longitudinal component contributions (dashed line), and the EWA result from taking the asymptotic formula [46] for the longitudinal scattering amplitude⁴ (dotted line). We see that the three curves coincide at high energies which indicates that the asymptotic behavior of the complete tree level result is correct. The dashed line is significantly below the solid line at lower energies, which shows that the signal from the transverse component contributions taken into account in the complete tree

level calculation is very important. The dotted line is much lower than the dashed line at low energies even they are all from the EWA approach with only the longitudinal component contributions taken into account. This is because that there are contributions of energy-independent terms contained in the dashed line which are not contained in the dotted line, and the energy-independent terms peak significantly in the low energy region due to the larger parton luminosities in the smaller M_{WW} region. To check the correctness of this explanation, we have calculated not only the M_{WW} distribution with a constant amplitude which shows the mentioned peak, but also the M_{WW} distributions for the two EWA curves with a very large f_W/Λ^2 , say $f_W/\Lambda^2 = 100 \text{ TeV}^{-2}$, with which the energy-independent terms are unimportant. Indeed, the two obtained curves in this case almost completely coincide, and the peak is shifted significantly to the high energy region. Finally, we note that for the values of the anomalous couplings relevant to the bounds given in Eqs. (29) and (30), the unitarity condition is well respected, so that our full $2 \rightarrow 4$ calculation is justified. Furthermore, since in our full $2 \rightarrow 4$ calculation, we keep track on the polarization states of the final state V bosons, we can also predict the kinematical distributions of the final state leptons. As an example, we show in Fig. 6 the distribution of the invariant mass of the di-leptons from the decay of the final state W^+ bosons produced via $pp \rightarrow W^+W^+jj$ for various scenarios of the anomalous couplings. Examining in detail various kinematical distributions might help to distinguish various scenarios of new physics effect.

VII. CONCLUSIONS

We have examined the possibility of testing anomalous HVV couplings of a light Higgs boson with mass $115 \text{ GeV} \leq m_H \leq 300 \text{ GeV}$ at the LHC via various channels of VV scatterings. This type of tests are of special interest if the anomalous HVV couplings differ from that of the SM by a significant amount so that the direct detection of the Higgs resonance is difficult. The study includes two types of anomalous HVV couplings, namely the anomalous HVV couplings from the nonlinear dimension-3 operator [11] and anomalous HVV couplings from the linearly realized dimension-6 operators [12,13]. The gold-plated pure leptonic modes are chosen for detecting the final state weak bosons. To reduce the various kinds of backgrounds, we impose the kinematical cuts suggested in Ref. [14,17]. The calculations are carried out numerically for the full cross sections of $pp \rightarrow VVjj$ including both the signals and the backgrounds under

⁴It only contains terms proportional to E^4 or E^2 . The E^0 contribution is not included.

the kinematical cuts, and we take into account only the statistical uncertainties in this calculation. The results show that, with a sufficiently high integrated luminosity, such as 300 fb^{-1} (3-year full luminosity run of the LHC), the tests of the anomalous HVV couplings can be rather sensitive. We note that to further discriminate the effect of the anomalous HVV coupling from that of a strongly interacting EWSB sector with no light resonance will eventually demand a multi-channel analysis at the LHC by searching for the light Higgs resonance through all possible on-shell production channels including gluon-gluon fusion. Once the light Higgs resonance is confirmed, VV scatterings, especially the W^+W^+ channel, can provide rather sensitive tests of various anomalous HVV couplings for probing the EWSB mechanism.

In the nonlinearly realized Higgs sector [11], the leading anomalous HVV coupling (κ) comes from the dimension-3 operator $\frac{1}{2}\kappa\nu H D_\mu \Sigma^\dagger D^\mu \Sigma$. The difference $\Delta\kappa \equiv \kappa - 1$ represents the deviation from the SM value $\kappa = 1$. Our calculation shows that the most sensitive channel for testing this anomalous coupling is $pp \rightarrow W^+W^+jj \rightarrow \ell^+\nu\ell^+\nu jj$. We see from Table III that the LHC can constrain $\Delta\kappa$ to the range $-0.3 \leq \Delta\kappa \leq 0.2$ if no anomalous coupling effect is detected in the channel $pp \rightarrow \ell^+\nu\ell^+\nu jj$. For the comparison, several possible tests of $\Delta\kappa$ in the high energy collider experiments are also discussed in Sec. III. A summary of all the constraints considered in Sec. III is listed in Table XIII.

In the linearly realized Higgs sector [13], the leading anomalous HVV couplings arise from a set of dimension-6 operators, $\frac{f_W}{\Lambda^2}\mathcal{O}_W$, $\frac{f_{WW}}{\Lambda^2}\mathcal{O}_{WW}$, $\frac{f_B}{\Lambda^2}\mathcal{O}_B$, and $\frac{f_{BB}}{\Lambda^2}\mathcal{O}_{BB}$, as shown in Eq. (18). The anomalous HWW and HZZ couplings are expressed in Eq. (21) in terms of the Lorentz-invariant form factors $g_{HWW}^{(1)}$, $g_{HWW}^{(2)}$, $g_{HZZ}^{(1)}$ and $g_{HZZ}^{(2)}$ which are connected to the above anomalous coupling constants f_W , f_{WW} , f_B , and f_{BB} via Eq. (22). These anomalous coupling constants are constrained by the precision electroweak data, the triple gauge coupling data, and the requirement of the unitarity of the S -matrix. Such constraints on the coupling constants f_n are give in Eqs. (23)–(27). The corresponding constraints on $g_{HWW}^{(1)}$, $g_{HWW}^{(2)}$, $g_{HZZ}^{(1)}$, and $g_{HZZ}^{(2)}$ are shown in Eq. (28) which restricts these anomalous couplings to be of $O(10^{-1}) - O(1)$. Our calculation shows that the anomalous HWW couplings can be sensitively tested via $pp \rightarrow W^+W^+jj \rightarrow \ell^+\nu\ell^+\nu jj$. Since there are several anomalous couplings from the dim-6 operators contributing to the VV scatterings, the analysis of the LHC sensitivity is more complicated than in the nonlinearly realized case. If the anomalous couplings are of the same order of magnitude, the interferences

depending on their relative signs could be significant. In this study, we made a single parameter analysis, i.e., assuming only one of the anomalous coupling constants is dominant at a time. Detailed calculations showed that the contributions of f_B and f_{BB} to the most sensitive $pp \rightarrow W^+W^+jj \rightarrow W^+W^+\ell^+\nu\ell^+\nu jj$ channel are very small even if they are of the same order of magnitude as other anomalous coupling constants. So, f_B and f_{BB} are not useful in our analysis. We then analyzed the two parameters f_W and f_{WW} separately. The 1σ and 2σ bounds on these two anomalous couplings via the most sensitive channel $pp \rightarrow W^+W^+jj \rightarrow W^+W^+\ell^+\nu\ell^+\nu jj$ are listed in Eqs. (29) and (30), and the corresponding bounds on the anomalous couplings $g_{HVV}^{(i)}$, $i = 1, 2$ are given in Eq. (32). These bounds are stronger than that obtained from Higgs production via weak boson fusion given in Ref. [6]. They are also complementary to the bounds on $g_{HZZ}^{(1)}$ and $g_{HZZ}^{(2)}$ at the Linear Collider (LC), as given in Ref. [3]. A summary of all the constraints considered in Sec. IV is displayed in Table XIV.

In summary, we find that *VV scatterings are not only important for probing the strongly interacting electroweak symmetry breaking mechanism when there is no light Higgs boson, but also valuable for sensitively testing of the anomalous HVV couplings (especially anomalous HWW coupling) at the LHC when there is a light Higgs boson in the mass range of 115–300 GeV*. This further supports the “no-lose” theorem [9] for the LHC to decisively probe the electroweak symmetry mechanism.

Acknowledgements We would like to thank Jens Erler and Peter B. Renton for discussing the electroweak precision data, Tao Han for interesting discussions and for providing related calculation codes; and Dieter Zeppenfeld for discussing the weak boson physics. BZ and YPK are supported by the National Natural Science Foundation of China (under Grant 90103008) and Foundation of Fundamental Research of Tsinghua University; HJH and CPY are supported by the Department of Energy of USA under Grant DEFG0393ER40757, and the National Science Foundation of USA under Grant PHY-0100677, respectively.

[1] R. Dashen and H. Neuberger, Phys. Rev. Lett. **50**, 1897 (1993); J. Kuti, L. Lin, and Y. Shen, *ibid.* **61**, 678 (1998); M. Lüscher and P. Weisz, Nucl. Phys. **B 318**,

- 705 (1989).
- [2] L. Susskind, Phys. Rev. D **20**, 2619 (1979); G. 'tHooft, in Proceedings of *Recent Development in Gauge Theories*, New York, U.S.A., 1979.
- [3] E.g., V. Barger, K. Cheung, A. Djouadi, B.A. Kniel, and P. M. Zerwas, Phys. Rev. D **49**, 79 (1994); M. Kramer, J. Kuhn, M. L. Stong and P. M. Zerwas, Z. Phys. C **64**, 21 (1994); K. Hagiwara and M. Stong, Z. Phys. C **62**, 99 (1994); J.F. Gunion, T. Han, and R. Sobey, Phys. Lett. B **429**, 79 (1995); K. Hagiwara, S. Ishihara, J. Kamoshita, and B.A. Kniel, Eur. Phys. J. **14**, 457 (2000).
- [4] O. J. P. Éboli, M. C. Gonzalez-Garcia, S. M. Lietti, and S. F. Novaes, Phys. Lett. B **478**, 199 (2000).
- [5] F. de Campos, M. C. Gonzalez-Garcia, S. M. Lietti, S. F. Novaes, and R. Rosenfeld, Phys. Lett. B **435**, 407 (1998).
- [6] D. Zeppenfeld, hep-ph/0203123, Snowmass contribution; T. Plehn, D. Rainwater, D. Zeppenfeld, Phys. Rev. Lett. **88**, 051801 (2002).
- [7] H.-J. He, Y.-P. Kuang, C.-P. Yuan, B. Zhang, Phys. Lett. B **554**, 64 (2003) [hep-ph/0211229].
- [8] R. S. Chivukula, M. J. Dugan and M. Golden, Phys. Lett. B **336**, 62 (1994).
- [9] M. S. Chanowitz and M. K. Gaillard, Nucl. Phys. B **261** (1985) 379; Michael S. Chanowitz, Lecture at Zuoz Summer School [hep-ph/9812215] and references therein.
- [10] H.-J. He, Y.-P. Kuang and C.-P. Yuan, Phys. Rev. D **55**, 3038 (1997); Phys. Lett. B **382**, 149 (1996).
- [11] R. Sekhar Chivukula and V. Koulovassilopoulos, Phys. Lett. B **309**, 371 (1993).
- [12] W. Buchmüller and D. Wyler, Nucl. Phys. B **268**, 621 (1986); C. J. C. Burgess and H. J. Schnitzer, Nucl. Phys. B **228**, 454 (1983); C. N. Leung, S. T. Love and S. Rao, Z. Phys. **31**, 433 (1986); A. De Rújula, M. B. Gavela, P. Hernández and E. Massó, Nucl. Phys. B **384**, 3 (1992).
- [13] For a review, M. C. Gonzalez-Garcia, Int. J. Mod. Phys. A **14**, 3121 (1999).
- [14] J. Bagger, V. Barger, K. Cheung, J. Gunion, T. Han, G. Ladinsky, R. Rosenfeld, and C.-P. Yuan, Phys. Rev. D **49**, 1246 (1994).
- [15] C.-P. Yuan "Proposals for Studying TeV $W_L W_L \rightarrow W_L W_L$ Interactions Experiments", [hep-ph/9712513], in *Perspectives on Higgs Physics*, second edition, edited by G. L. Kane (World Scientific, Singapore).
- [16] J. Pumplin, D.R. Stump, J. Huston, H.L. Lai, P. Nadolsky, W.K. Tung, JHEP **0207**,012 (2002).
- [17] J. Bagger, V. Barger, K. Cheung, J. Gunion, T. Han, G. Ladinsky, R. Rosenfeld, and C.-P. Yuan, Phys. Rev. D **52**, 3878 (1995);
- [18] M. S. Chanowitz and M. K. Gaillard, Phys. Lett. B **142**, 85 (1984); G. L. Kane, W. W. Repko, W. R. Rolnik, Phys. Lett. B **148**,367 (1984); S. Dawson, Nucl. Phys. B **249**,427 (1985).
- [19] E. Boos, H.-J. He, W. Kilian, A. Pukhov, C.-P. Yuan, and P.M. Zerwas, Phys. Rev. D **57**, 1553 (1998); Phys. Rev. D **61**, 077901 (2000).
- [20] A. Manohar and H. Georgi, Nucl. Phys. B **234**, 189 (1984).
- [21] M.E. Peskin and T. Takeuchi, Phys. Rev. D **46**, 381 (1992).
- [22] T. Appelquist and C. Bernard, Phys. Rev. D **22**, 200 (1980); A. C. Longhitano, Nucl. Phys. B **188**, 118 (1981).
- [23] E.g., S. Dawson and G. Valencia, Nucl. Phys. B **439**, 3 (1995).
- [24] H. Georgi, Ann. Rev. Nucl. & Part. Sci. **43**, 209 (1994), and references therein.
- [25] Particle Data Group (K. Hagiwara *et al.*), Phys. Rev. D **66**, 010001 (2002).
- [26] B. A. Dobrescu and C. T. Hill, Phys. Rev. Lett. **81**, 2634 (1998); R. S. Chivukula, B. A. Dobrescu, H. Georgi, and C. T. Hill, Phys. Rev. D **59**, 075003 (1999); H.-J. He, C. T. Hill, and T. Tait, Phys. Rev. D **65**, 055006 (2002); H.-J. He, T. Tait, and C.-P. Yuan, Phys. Rev. D **62**, 011702 (2000) (R).
- [27] J. Bagger, A. F. Falk and M. Swartz, Phys. Rev. Lett. **84**, 1385 (2000); R. S. Chivukula, C. Holbling and N. Evans, Phys. Rev. Lett. **85**, 511 (2000); C. Kolda and H. Murayama, JHEP **0007**, 035 (2000); M. E. Peskin and J. D. Wells, Phys. Rev. D **64**, 093003 (2001).
- [28] H.-J. He, N. Polonsky and S. Su, Phys. Rev. D **64**, 053004 (2001) [hep-ph/0102144].
- [29] R. Sekhar Chivukula and C. Holbling, Snowmass contribution [hep-ph/0110214].
- [30] M. S. Chanowitz, Phys. Rev. D **66**, 073002 (2002) [hep-ph/0207123].
- [31] E.g., G. A. Miller and A. W. Thomas, hep-ex/0204007; S. Davidson, hep-ph/0209316.
- [32] J. Erler, private communications, hep-ph/0005084 and review at <http://pdg.lbl.gov>; P. Langacker, J.Phys. G **29**, 1 (2003) [hep-ph/0211065].
- [33] M. W. Gr newald, talk at ICHEP, Amsterdam, July 24-31, 2002 [hep-ex/0210003], and LEP Electroweak Working Group, <http://www.cern.ch/LEPEWWG>; see also, P. B. Renton, Rept. Prog. Phys. **65**, 1271 (2002) [hep-ph/0206231].
- [34] For an updated comprehensive review, C. T. Hill and E. H. Simmons, hep-ph/0203079.
- [35] E. Malkawi and C.-P. Yuan, Phys. Rev. D **52** (1995) 472; F. Larios, M.A. Perez and C.-P. Yuan, Phys. Lett. B **457** (1999) 334.
- [36] H.-J. He, Y.-P. Kuang and C.-P. Yuan, Phys. Rev. D **55**, 3038 (1997) [hep-ph/9611316]; Phys. Lett. B **382**, 149 (1996) [hep-ph/9604309]; and review in DESY-97-056 [hep-ph/9704276].
- [37] ALEPH, DELPHI, L3 and OPAL (The LEP working group for Higgs searches), talk presented at 2001 International Symposium on Lepton and Photon Interactions at High Energies, Rome, 2001, hep-ex/0107029; U. Schwickerath, hep-ph/0205126.
- [38] P. Agrawal, hep-ph/0011347.
- [39] V. Drollinger and A. Sopczak, hep-ph/0102342.
- [40] F. Gianotti, *et al.*, CERN-TH/2002-078, hep-ph/0204087.
- [41] D. Zeppenfeld, hep-ph/0203123.

- [42] K. Hagiwara, S. Ishihara, R. Szalapski and D. Zeppenfeld, Phys. Lett. B **283**, 353 (1992); Phys. Rev. D **48**, 2182 (1993).
- [43] S. Alam, S. Dawson, R. Szalapski, Phys. Rev. D **57**, 1577 (1998); K. Hagiwara, S. Matsumoto R. Szalapski, Phys. Lett. B **357**, 411 (1995).
- [44] B. Abbott *et al.*, D0 Collaboration, Phys. Rev. D **58**, 031102 (1998).
- [45] ALEPH Collaboration, R. Barate *et al.*, Phys. Lett. B **422**, 369 (1998); DELPHI Collaboration, P. Abreu *et al.*, Phys. Lett. B **423**, 194 (1998); L3 Collaboration, M. Acciari *et al.*, Phys. Lett. B **413**, 176 (1998); OPAL Collaboration, K. Ackerstaff *et al.*, Eur. Phys. J. **C2**, 597 (1998).
- [46] G.J. Gounaris, J. Layssac, and F.M. Renard, Phys. Lett. B **332**, 146 (1994); G.J. Gounaris, J. Layssac, J.E. Pascalis, and F.M. Renard, Z. Phys. C **66**, 619 (1995).

TABLES

Table I. The 95% C.L. limits on $\Delta\kappa$ for typical values of new physics scale Λ and Higgs mass m_H .

m_H (GeV)	Λ (TeV)		
	1	10	100
115	$-0.15 \leq \Delta\kappa \leq 0.23$	$-0.069 \leq \Delta\kappa \leq 0.12$	$-0.045 \leq \Delta\kappa \leq 0.08$
300	$-0.074 \leq \Delta\kappa \leq 0.60$	$0.027 \leq \Delta\kappa \leq 0.24$	$0.016 \leq \Delta\kappa \leq 0.15$
800	(excluded)	$0.20 \leq \Delta\kappa \leq 0.45$	$0.11 \leq \Delta\kappa \leq 0.26$

Table II. Cross section σ (in fb) in the W^+W^+ channel for $m_H = 115$ GeV and various values of $\Delta\kappa$ contributed by different polarizations of W^+W^+ .

$\Delta\kappa$	σ_{all}	σ_{LL}	σ_{LT}	σ_{TT}
0.0	1.1	0.02	0.2	0.8
0.4	4.1	3.0	0.3	0.8

Table III. Number of events with an integrated luminosity of 300 fb^{-1} at the LHC for $pp \rightarrow W^\pm W^\pm jj \rightarrow l^\pm \nu(\bar{\nu}) l^\pm \nu(\bar{\nu}) jj$ ($l^\pm = e^\pm$ or μ^\pm) with various values of m_H and $\Delta\kappa$ ($\Delta\kappa = 0$ corresponds to the SM). The values of $N_S/\sqrt{N_S + N_B}$ are shown in the parentheses.

$pp \rightarrow W^+W^+jj \rightarrow l^+\nu l^+\nu jj$											
m_H (GeV)	$\Delta\kappa$										
	-1.0	-0.6	-0.3	0.0	0.2	0.3	0.4	0.5	0.6	0.7	
115	62 (6.0)	48 (4.8)	27 (2.3)	15	24 (1.8)	37 (3.6)	58 (5.6)	—	—	—	
130	62 (6.0)	48 (4.8)	27 (2.3)	15	24 (1.8)	37 (3.6)	57 (5.5)	—	—	—	
200	62 (6.0)	48 (4.8)	28 (2.5)	15	22 (1.5)	33 (3.1)	52 (5.1)	78 (7.1)	—	—	
300	61 (5.9)	49 (4.9)	30 (2.7)	16	20 (1.1)	29 (2.6)	43 (4.3)	65 (6.2)	95 (8.2)	136 (10.4)	

$pp \rightarrow W^-W^-jj \rightarrow l^-\bar{\nu} l^-\bar{\nu} jj$											
m_H (GeV)	$\Delta\kappa$										
	-1.0	-0.6	-0.3	0.0	0.2	0.3	0.4	0.5	0.6	0.7	
115	13	10	6	3	4	6	9	—	—	—	
130	13	10	6	3	4	6	9	—	—	—	
200	13	10	6	3	4	6	8	11	—	—	
300	13	10	6	4	4	5	7	10	14	19	

Table IV. Number of events with an integrated luminosity of 300 fb^{-1} at the LHC for $pp \rightarrow W^+W^-jj \rightarrow l^+\nu l^-\nu jj$ ($l^\pm = e^\pm$ or μ^\pm) with various values of m_H and $\Delta\kappa$ ($\Delta\kappa = 0$ corresponds to the SM). The values of $N_S/\sqrt{N_S + N_B}$ are shown in the parentheses.

$m_H(\text{GeV})$	-1.0	-0.6	-0.3	0.0	$\Delta\kappa$ 0.2	0.3	0.4	0.5	0.6	0.7
115	19(3.4)	14(2.7)	8(1.4)	4	7(1.1)	11(2.1)	17(3.2)	–	–	–
130	19(3.4)	14(2.7)	8(1.4)	4	7(1.1)	11(2.1)	17(3.2)	–	–	–
200	19(3.4)	14(2.7)	8(1.4)	4	8(1.1)	12(2.3)	19(3.4)	29(4.6)	–	–
300	19(3.4)	14(2.7)	7(1.1)	4	9(1.7)	14(2.7)	23(4.0)	34(5.1)	48(6.4)	69(7.8)

Table V. Number of events with an integrated luminosity of 300 fb^{-1} at the LHC for $pp \rightarrow ZW^\pm jj \rightarrow l^+l^-l^\pm\nu(\bar{\nu})jj$ ($l^\pm = e^\pm$ or μ^\pm) with various values of m_H (in GeV) and $\Delta\kappa$ ($\Delta\kappa = 0$ corresponds to the SM).

$pp \rightarrow ZW^+jj \rightarrow l^+l^-l^+\nu jj$											
$m_H(\text{GeV})$	-1.0	-0.6	-0.3	0.0	$\Delta\kappa$ 0.2	0.3	0.4	0.5	0.6	0.7	
115	9	7	4	2	3	5	7	–	–	–	
130	9	7	4	2	3	5	7	–	–	–	
200	9	7	4	2	3	4	6	10	–	–	
300	9	7	4	2	3	4	5	9	12	16	

$pp \rightarrow ZW^-jj \rightarrow l^+l^-l^-\bar{\nu} jj$											
$m_H(\text{GeV})$	-1.0	-0.6	-0.3	1.0	$\Delta\kappa$ 0.2	0.3	0.4	0.5	0.6	0.7	
115	4	3	2	1	1	2	3	–	–	–	
130	4	3	2	1	1	2	3	–	–	–	
200	4	3	2	1	1	2	3	4	–	–	
300	4	3	2	1	1	2	2	4	5	7	

Table VI. Number of events with an integrated luminosity of 300 fb^{-1} at the LHC for $pp \rightarrow ZZjj \rightarrow l^+l^-l^+l^-(\nu\bar{\nu})jj$ ($l^\pm = e^\pm$ or μ^\pm) with various values of m_H (in GeV) and $\Delta\kappa$ in the nonlinearly realized NSHM ($\Delta\kappa = 0$ corresponds to the SM).

$pp \rightarrow ZZjj \rightarrow l^+l^-l^+l^-jj$										
$m_H(\text{GeV})$	-1.0	-0.6	-0.3	0.0	$\Delta\kappa$	0.3	0.4	0.5	0.6	0.7
115	9	8	5	4	5	6	8	–	–	–
130	9	8	5	4	5	6	8	–	–	–
200	9	8	5	4	5	7	9	13	–	–
300	9	7	5	4	6	9	12	17	24	32

$pp \rightarrow ZZjj \rightarrow l^+l^- \nu\bar{\nu}jj$										
$m_H(\text{GeV})$	-1.0	-0.6	-0.3	0.0	$\Delta\kappa$	0.3	0.4	0.5	0.6	0.7
115	5	4	2	0	1	3	5	–	–	–
130	5	4	2	0	1	3	5	–	–	–
200	5	4	2	0	1	3	5	8	–	–
300	5	4	2	0	1	3	6	9	14	20

Table VII. $B(H \rightarrow \gamma\gamma)$, in the unit of 10^{-3} , as a function of $|\kappa|$ for various m_H .

$m_H(\text{GeV})$	0.6	0.7	0.8	0.9	0.95	$ \kappa $	1.05	1.1	1.2	1.3	1.4
110	5.0	4.1	2.6	2.1	2.0	1.9	1.8	1.8	1.7	1.6	1.6
120	5.0	6.1	3.6	2.6	2.4	2.2	2.1	2.0	1.8	1.7	1.6
130	4.6	5.7	6.3	3.0	2.6	2.3	2.1	1.9	1.6	1.5	1.3

Table VIII. $B(\kappa) \equiv B(H \rightarrow WW^*)$ as a function of $|\kappa|$ for various m_H .

$m_H(\text{GeV})$	0.6	0.7	0.8	0.9	0.95	$ \kappa $	1.05	1.1	1.2	1.3	1.4
110	0.013	0.018	0.024	0.03	0.033	0.037	0.040	0.044	0.052	0.061	0.069
120	0.048	0.064	0.082	0.10	0.11	0.12	0.13	0.14	0.17	0.19	0.21
130	0.12	0.16	0.20	0.24	0.26	0.28	0.30	0.32	0.35	0.39	0.42
150	0.48	0.55	0.60	0.65	0.67	0.68	0.70	0.71	0.74	0.76	0.78
170	0.95	0.95	0.96	0.96	0.96	0.97	0.97	0.97	0.97	0.97	0.97

Table IXA. Number of events with an integrated luminosity 300 fb^{-1} at the LHC for the process $pp \rightarrow W^{\pm}W^{\pm} \rightarrow l^{\pm}\nu l^{\pm}\nu jj$ ($l^{\pm} = e^{\pm}$ or μ^{\pm}) in the linearly realized effective Lagrangian with various values of m_H and f_W/Λ^2 . The values of $N_S/\sqrt{N_S + N_B}$ are shown in the parentheses.

$pp \rightarrow W^+W^+jj \rightarrow l^+\nu l^+\nu jj$											
$m_H(\text{GeV})$	$f_W/\Lambda^2 \text{ (TeV}^{-2}\text{)}$										
	-4.0	-3.0	-2.0	-1.4	-1.0	0.0	0.85	1.2	2.0	3.0	4.0
115	117(9.4)	72(6.7)	38(3.7)	26(2.2)	20(1.1)	15	20(1.1)	25(2.0)	42(4.2)	78(7.1)	129(10)
130	118(9.5)	72(6.7)	38(3.7)	26(2.2)	20(1.1)	15	20(1.1)	25(2.0)	42(4.2)	78(7.1)	130(10)
200	119(9.5)	73(6.8)	38(3.7)	26(2.2)	20(1.1)	15	20(1.1)	25(2.0)	42(4.2)	79(7.2)	132(10)
300	121(9.6)	75(6.9)	39(3.8)	27(2.3)	21(1.3)	16	21(1.3)	26(2.2)	43(4.3)	80(7.3)	134(10)

$pp \rightarrow W^-W^-jj \rightarrow l^-\bar{\nu} l^-\bar{\nu} jj$											
$m_H(\text{GeV})$	$f_W/\Lambda^2 \text{ (TeV}^{-2}\text{)}$										
	-4.0	-3.0	-2.0	-1.4	-1.0	0.0	0.85	1.2	2.0	3.0	4.0
115	23	14	7	5	4	3	4	5	8	15	25
130	23	14	7	5	4	3	4	5	8	15	25
200	23	14	7	5	4	3	4	5	8	15	26
300	24	15	8	5	4	4	4	5	8	16	26

Table IXB. Number of events with an integrated luminosity 300 fb^{-1} at the LHC for the process $pp \rightarrow W^{\pm}W^{\pm} \rightarrow l^{\pm}\nu l^{\pm}\nu jj$ ($l^{\pm} = e^{\pm}$ or μ^{\pm}) in the linearly realized effective Lagrangian with various values of m_H and f_{WW}/Λ^2 . The values of $N_S/\sqrt{N_S + N_B}$ are shown in the parentheses.

$pp \rightarrow W^+W^+jj \rightarrow l^+\nu l^+\nu jj$										
$m_H(\text{GeV})$	$f_{WW}/\Lambda^2 \text{ (TeV}^{-2}\text{)}$									
	-4.0	-3.0	-2.2	-1.6	0.0	1.6	2.2	3.0	4.0	
115	47(4.7)	33(3.1)	25(2.0)	19(0.9)	15	20(1.1)	26(2.2)	33(3.1)	48(4.8)	
130	48(4.8)	33(3.1)	25(2.0)	19(0.9)	15	20(1.1)	26(2.2)	34(3.1)	49(4.9)	
200	49(4.9)	34(3.3)	25(2.0)	19(0.9)	15	20(1.1)	26(2.2)	35(3.4)	50(4.9)	
300	51(5.0)	35(3.4)	26(2.2)	20(1.1)	16	21(1.3)	27(2.3)	36(3.5)	52(5.1)	

$pp \rightarrow W^-W^-jj \rightarrow l^-\bar{\nu} l^-\bar{\nu} jj$										
$m_H(\text{GeV})$	$f_{WW}/\Lambda^2 \text{ (TeV}^{-2}\text{)}$									
	-4.0	-3.0	-2.2	-1.6	0.0	1.6	2.2	3.0	4.0	
115	9	6	5	4	3	4	5	6	9	
130	9	6	5	4	3	4	5	7	10	
200	10	7	5	4	3	4	5	7	10	
300	10	7	5	4	4	4	5	7	10	

Table X. Number of events with the integrated luminosity 300 fb^{-1} at the LHC for the process $pp \rightarrow W^+W^-jj \rightarrow l^+\nu l^-\nu jj$ ($l^{\pm} = e^{\pm}$ or μ^{\pm}) in the linearly realized effective Lagrangian with various values of m_H and F_W/Λ^2 . The values of $N_S/\sqrt{N_S + N_B}$ are shown in the parentheses.

$m_H(\text{GeV})$	$f_W/\Lambda^2 \text{ (TeV}^{-2}\text{)}$								
	-4.0	-3.0	-2.0	-1.0	0.0	1.0	2.0	3.0	4.0
115	35	21	10	5	4	6	12	23	38
130	35	21	10	5	4	6	12	23	38
200	36	21	10	5	4	6	12	23	39
300	37	22	11	5	4	6	13	24	40

Table XI. Number of events with the integrated luminosity 300 fb^{-1} at the LHC for the process $pp \rightarrow ZZjj \rightarrow l^+l^-l^+l^- (l^+l^- \nu \bar{\nu})jj$ ($l^\pm = e^\pm$ or μ^\pm) in the linearly realized effective Lagrangian with various values of m_H and F_W/Λ^2 .

$pp \rightarrow ZZjj \rightarrow l^+l^- \nu \bar{\nu} jj$										
$m_H(\text{GeV})$	$f_W/\Lambda^2 (\text{TeV}^{-2})$					$f_W/\Lambda^2 (\text{TeV}^{-2})$				
	-4.0	-3.0	-2.0	-1.0	0.0	1.0	2.0	3.0	4.0	
115	10	6	2	1	0	1	3	6	11	
130	10	6	2	1	0	1	3	6	11	
200	10	6	2	1	0	1	3	6	11	
300	10	6	2	1	0	1	3	6	12	

$pp \rightarrow ZZjj \rightarrow l^+l^-l^+l^- jj$										
$m_H(\text{GeV})$	$f_W/\Lambda^2 (\text{TeV}^{-2})$					$f_W/\Lambda^2 (\text{TeV}^{-2})$				
	-4.0	-3.0	-2.0	-1.0	0.0	1.0	2.0	3.0	4.0	
115	9	7	5	4	4	5	6	8	10	
130	9	7	5	4	4	5	6	8	10	
200	9	7	5	4	4	5	6	8	10	
300	9	7	5	4	4	5	6	8	11	

Table XII. Number of events with the integrated luminosity 300 fb^{-1} at the LHC for the process $pp \rightarrow ZW^\pm jj \rightarrow l^\pm \nu l^\pm jj$ ($l^\pm = e^\pm$ or μ^\pm) in the linearly realized effective Lagrangian with various values of m_H and F_W/Λ^2 .

$pp \rightarrow ZW^+ jj \rightarrow l^+l^-l^+\nu jj$										
$m_H(\text{GeV})$	$f_W/\Lambda^2 (\text{TeV}^{-2})$					$f_W/\Lambda^2 (\text{TeV}^{-2})$				
	-4.0	-3.0	-2.0	-1.0	0.0	1.0	2.0	3.0	4.0	
115	10	7	4	3	2	3	5	8	12	
130	10	7	4	3	2	3	5	8	12	
200	10	7	4	3	2	3	5	8	12	
300	10	7	4	3	2	3	5	8	12	

$pp \rightarrow ZW^- jj \rightarrow l^+l^-l^-\nu jj$										
$m_H(\text{GeV})$	$f_W/\Lambda^2 (\text{TeV}^{-2})$					$f_W/\Lambda^2 (\text{TeV}^{-2})$				
	-4.0	-3.0	-2.0	-1.0	0.0	1.0	2.0	3.0	4.0	
115	4	2	1	1	1	1	1	2	4	
130	4	2	1	1	1	1	1	2	4	
200	4	2	1	1	1	1	1	2	4	
300	4	2	1	1	1	1	1	2	4	

Table XIII. Summary of the 2σ constraints on the anomalous HVV coupling κ ($\equiv 1 + \Delta\kappa$) from the dimension-3 operator in the nonlinear Higgs sector studied in Sec. III.

Types of constraints	results	Places in the text
Precision EW data	regions shown in Fig. 2 and 3, Table I	Eq. (6)
Unitarity ($\sqrt{s}=2 \text{ TeV}$)	$0.5 < \kappa < 1.3$	Eq. (11)
W^+W^+ scattering	$-0.3 < \Delta\kappa < 0.2$	Eq. (13)
HV production ($m_H = 120 \text{ GeV}$)	$0 \leq \kappa \leq 1.6$	Eq. (14)
Higgs width ($m_H = 200 - 300 \text{ GeV}$)	$0.8 \leq \kappa \leq 1.2$	Eq. (15)
$B(H \rightarrow \gamma\gamma)$	Table VII	Sec. V.c
Higgs resonance ($m_H = 120 \text{ GeV}$)	$0.88 \leq R \leq 1.12$ [$R \equiv \kappa^2 B(\kappa)/B(\kappa=1)$], Table VIII	Eq. (16)

Table XIV. Summary of the 2σ constraints on the anomalous HVV coupling f_n/Λ^2 (in TeV^{-2}) associated with the dimension-6 operators [cf. Eqs. (17)–(19)] and the related form factors $g_{HVV}^{(1)}$ and $g_{HVV}^{(2)}$ (in TeV^{-1}) [cf. Eq. (22)] in the linearly realized Higgs sector studied in Sec. IV.

types of constraints	results	places in the text	
precision EW data	2-parameter fit at tree level: regions shown in Fig. 4	Fig. 4	
	1-parameter fit at 1-loop level: $-6 \leq \frac{f_{WWW}}{\Lambda^2} \leq 3, \quad -6 \leq \frac{f_W}{\Lambda^2} \leq 5, \quad -4.2 \leq \frac{f_B}{\Lambda^2} \leq 2.0,$ $-5.0 \leq \frac{f_{WW}}{\Lambda^2} \leq 5.6, \quad -17 \leq \frac{f_{BB}}{\Lambda^2} \leq 20$	Eq. (23)	
triple gauge coupling data	$-31 \leq \frac{(f_W + f_B)}{\Lambda^2} \leq 68$ (for $f_{WWW} = 0$),		
	$-41 \leq \frac{f_{WWW}}{\Lambda^2} \leq 26$ (for $f_W + f_b = 0$)	Eq. (24)	
LEP2 Higgs searches	$-7.5 \leq \frac{f_{WW(BB)}}{\Lambda^2} \leq 18$	Eq. (25)	
unitarity ($\sqrt{s}=2$ TeV)	$ \frac{f_b}{\Lambda^2} \leq 24.5, \quad \frac{f_W}{\Lambda^2} \leq 7.8, \quad \frac{f_{WWW}}{\Lambda^2} \leq 7.5,$		
	$-160 \leq \frac{f_{BB}}{\Lambda^2} \leq 197, \quad \frac{f_{WW}}{\Lambda^2} \leq 39.2$	Eq. (27)	
W^+W^+ scattering	1σ	2σ	
	$-1.0 < \frac{f_W}{\Lambda^2} < 0.85$	$-1.4 < \frac{f_W}{\Lambda^2} \leq 1.2$	Eq. (28)
	$-1.6 < \frac{f_{WW}}{\Lambda^2} < 1.6$	$-2.2 \leq \frac{f_{WW}}{\Lambda^2} < 2.2$	Eq. (29)
or			
	$-0.026 < g_{HWW}^{(1)} < 0.022$	$-0.036 < g_{HWW}^{(1)} \leq 0.031$	
	$-0.026 < g_{HZZ}^{(1)} < 0.022$	$-0.036 < g_{HZZ}^{(1)} \leq 0.031$	
	$-0.014 < g_{HZ\gamma}^{(1)} < 0.012$	$-0.020 < g_{HZ\gamma}^{(1)} \leq 0.017$	
	$-0.083 < g_{HWW}^{(2)} < 0.083$	$-0.11 \leq g_{HWW}^{(2)} < 0.11$	
	$-0.032 < g_{HZZ}^{(2)} < 0.032$	$-0.044 \leq g_{HZZ}^{(2)} < 0.044$	
	$-0.018 < g_{HZ\gamma}^{(2)} < 0.018$	$-0.024 \leq g_{HZ\gamma}^{(2)} < 0.024$	Eqs. (31)

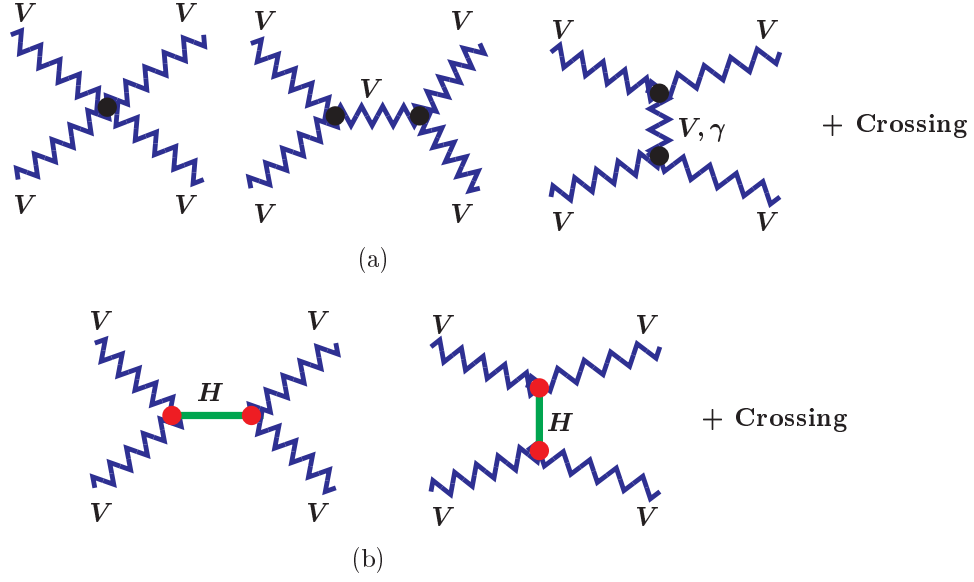


FIG. 1. Illustration of Feynman diagrams for $V_L V_L$ scatterings in the SM: (a) diagrams contributing to $T(V, \gamma)$, (b) diagrams contributing to $T(H)$.

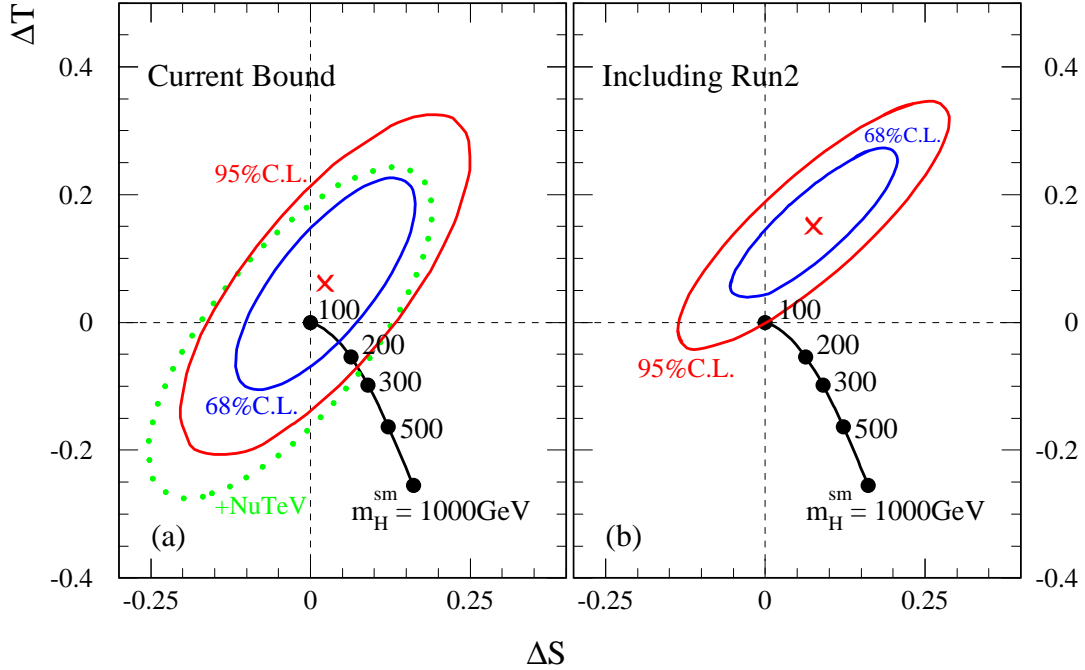


FIG. 2. $\Delta S - \Delta T$ contours (a) from the current precision electroweak data, and (b) from including the expected Tevatron Run-2 measurement of m_W and m_t (assuming the current central values of m_W and m_t with an error of 20 MeV and 2 GeV, respectively). Here, we have set $m_H^{\text{ref}} = 100 \text{ GeV}$ and $\Delta U = 0$ in the fit.

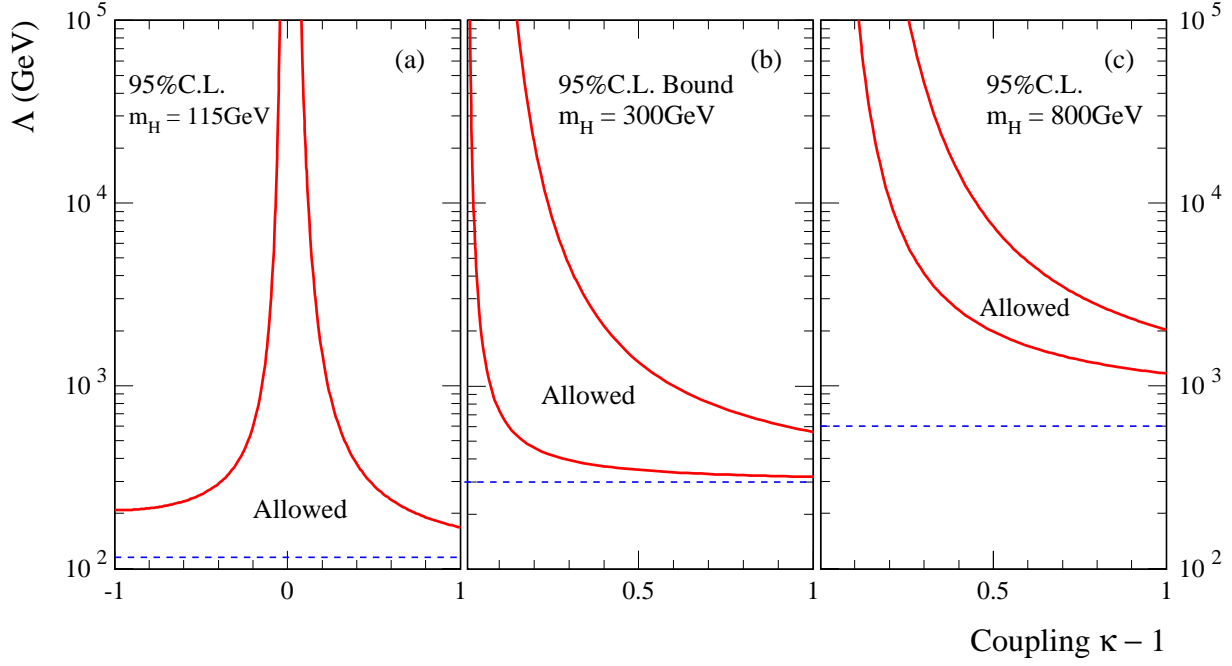


FIG. 3. Constraints on the new physics scale Λ as a function of the anomalous coupling $\Delta\kappa \equiv \kappa - 1$. The regions below the solid curves and above the dashed lines [(a)-(b)] or between the two solid curves [(c)-(d)] are allowed at the 95% C.L. The dashed lines indicate the value of $m_H^{\text{ref}} = m_H$.

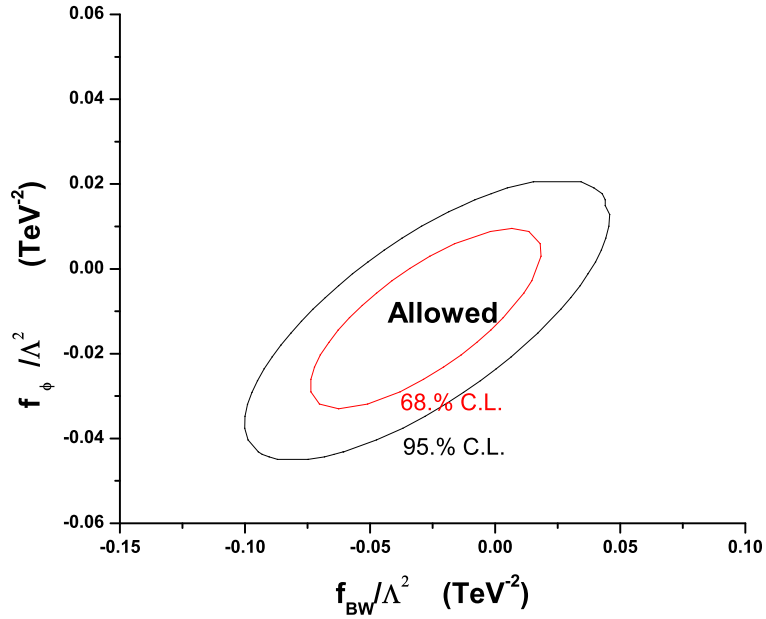


FIG. 4. 68% and 95% C.L. bounds on f_{BW}/Λ^2 and $f_{\Phi,1}/\Lambda^2$ (in units of TeV^{-2}) from the tree level formulas of ΔS and ΔT [40] and the ΔS - ΔT bounds given in Fig. 2(a).

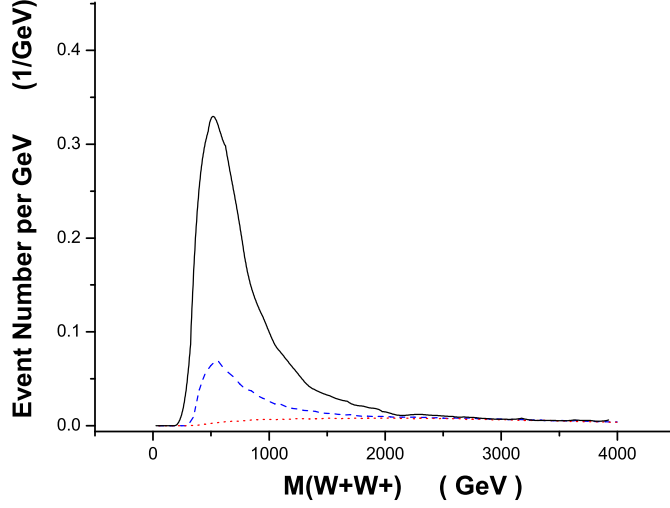


FIG. 5. Invariant mass distributions in the W^+W^+ channel for $m_H = 115$ GeV with $f_W/\Lambda^2 = f_B/\Lambda^2 = 5 \text{ TeV}^{-2}$. The solid line is the result from the complete tree level calculation; the dashed line is the result from the EWA calculation containing only the W_L^+ contributions; the dotted line is the result from the EWA calculation containing only the W_L^+ contributions but taking the asymptotic formula for the amplitude given in Ref.[43].

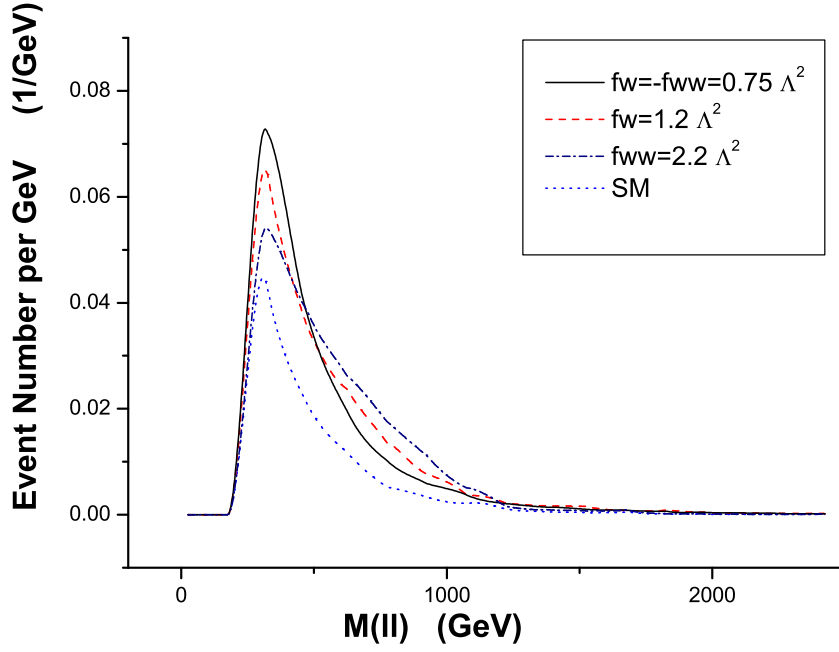


FIG. 6. Invariant mass distribution of the di-leptons from the decay of W^+ bosons produced at the LHC via $pp \rightarrow W^+W^+jj$ for $m_H = 115$ GeV with the 2σ values $f_W/\Lambda^2 = -f_{WW}/\Lambda^2 = 0.75 \text{ TeV}^{-2}$ [Eq. (31)] (solid line), $f_W/\Lambda^2 = 1.2 \text{ TeV}^{-2}$, $f_{WW}/\Lambda^2 = 0$ [Eq. (29)] (dashed line), $f_{WW}/\Lambda^2 = 2.2 \text{ TeV}^{-2}$, $f_W/\Lambda^2 = 0$ [Eq. (30)] (dashed-dotted line), and the SM (dotted line).